1

ZIRCONIUM PHOSPHATE NANOPARTICLES AND THEIR EXTRAORDINARY PROPERTIES

Abraham Clearfield and Agustin Diaz
Department of Chemistry, Texas A&M University, College Station, TX, USA

1.1 INTRODUCTION

The first report of a crystalline form of zirconium phosphate was in 1964. Up to that time, only an amorphous white fine powder was known. The transformation from the amorphous to crystalline is a slow process. It is therefore possible to control the size of the particles from very small, approximately 50 nm, to micro size and to large crystals. These particles are layered and exhibit the ability to exchange positively charged species for protons, to undergo intercalation behaviour and exfoliation of the layers. In addition, it has been shown that the surface of the particles may be functionalized by bonding to silanes, isocyanates and epoxides. By first replacing the surface protons by Zr^{4+} or Sn^{4+}, bonding may be extended to include phosphates and phosphonic acids. Attachment of a functional group to the surface bonding ligands including the phosphates or phosphonic acids allows this large class of functionalized molecules to be utilized for a variety of applications. Because of the extraordinary properties of this compound, a great variety of potential and realized uses have been invoked. As a result, from 1964 to the present, more than 10,000 scientific papers have been published describing the chemistry and applications of this remarkable compound. This phenomenon continues as every year a few hundred new papers appear in the chemical literature. Among the many uses in addition to ion exchange are catalysis, polymer composites, proton conduction, drug delivery and many more, as will be described in this chapter.

Tailored Organic–Inorganic Materials, First Edition. Edited by Ernesto Brunet, Jorge L. Colón and Abraham Clearfield.

1.2 SYNTHESIS AND CRYSTAL STRUCTURE OF α-ZIRCONIUM PHOSPHATE

We shall begin by describing the synthesis and structure of α-zirconium phosphate (α-ZrP), $Zr(O_3POH)_2 \cdot H_2O$. The addition of phosphoric acid to a soluble zirconium salt results in the precipitation of an amorphous white solid. This solid was observed to incorporate ions that may be in the solution. Interest in zirconium phosphate was keyed by the advent of nuclear energy. In swimming pool reactors, ionic species formed in the wastewater. These ions needed to be removed before the water could be reused. Because of the high temperature of the water and the radioactivity of the ions, organic resins were unsuitable for this purpose. It was felt that inorganic materials would serve the purpose and much work was concentrated on the amorphous zirconium phosphate [1, 2]. Unfortunately, the hot water hydrolysed the phosphate to hydroxide.

Our initial effort involved crystallizing the amorphous powder by adding excess phosphoric acid and heating the mix under reflux [3]. The single crystals for structure determination were prepared in 9 M H_3PO_4 in sealed tubes at 180°C. The availability of the single crystals resulted in the determination of their structure [4, 5].

α-ZrP is a layered compound as shown in Figure 1.1 and has the composition $Zr(O_3POH)_2 \cdot H_2O$ and an interlayer distance of 7.56 Å. The zirconium ions are arranged at the corners of a parallelogram with alternate Zr ions above and below the mean plane of the layer. The phosphate groups sit alternately above and below the mean plane of the layer with three oxygen atoms of the phosphate group bonding to three of the Zr^{4+} ions forming a triangle in half of the parallelogram. The Zr^{4+} are six coordinate with oxygen contributions from six phosphate groups in adjacent

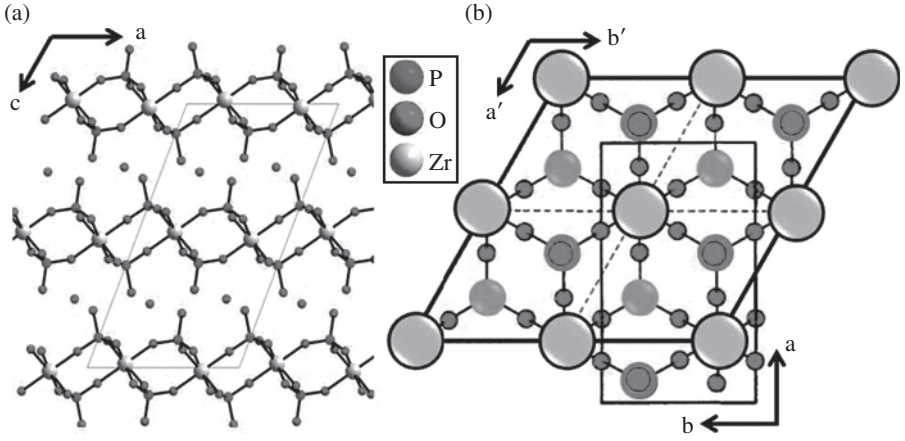

FIGURE 1.1 Schematic representation of α-ZrP viewed along the *b*-axis showing its unit cell and the formed layered structure (a) and along the *c*-axis (b) showing the surface of the layers. The view along the *c*-axis (b) is showing the relationship of the pseudo-hexagonal cell (black rectangle) to the true, monoclinic unit cell. The hydrogen atoms were omitted for clarity (Taken from: *Chem. Mater.* 2013, *25*, 723–728; DOI: 10.1021/cm303610v).

parallelograms. The P–OH groups form a double layer in the interlayer space. We shall refer to this compound as α-ZrP.

Before discussing any applications, some additional information on crystal growth and formation of the crystals is required. The solubility of the amorphous powder increases with an increase in concentration of phosphoric acid [6]. Thus, it is possible to control the growth of particles of α-ZrP by varying the concentration of the acid. In this way, we are able to grow nanoparticles of less than 100 nm through up to 4 μm-sized particles and single crystals [7]. In fact, at present, particles of about 50 nm in size and only a few layers thick have been obtained [8]. Table 1.1 shows the various ways that were used to control particle size of the zirconium phosphate by varying the concentration of phosphoric acid, use of a hydrothermal technique at temperatures from 120 to 200°C or addition of HF as a solubilizing agent [7].

Of course, there is also time and temperature control to consider. The HF forms a complex ZrF_6^{2-} that releases Zr^{4+} slowly at temperatures above 60°C. The decreased yield in the HF method results from increased solubility of the ZrF_6^{2-} ions. An example of crystal growth is shown by the electron micrograph patterns in Figure 1.2. The numbers indicate the concentration of phosphoric acid and the reflux time.

TABLE 1.1 The yield and typical particle length of α-zrp samples prepared

Sample	Yield (%)	Typical particle length (nm)
ZrP(3 M)[a]	96.4	50–100
ZrP(6 M)[a]	87.3	100–200
ZrP(9 M)[a]	85.8	100–200
ZrP(12 M)[a]	86.6	150–300
ZrP(HT3 M-200-5)[b]	85.6	100–200
ZrP(HT6 M-200-5)[b]	90.7	150–250
ZrP(HT9 M-200-5)[b]	98.0	150–250
ZrP(HT12 M-200-5)[b]	97.3	200–400
ZrP(HT3 M-200-24)[c]	89.3	300–500
ZrP(HT6 M-200-24)[c]	97.1	600–800
ZrP(HT9 M-200-24)[c]	96.0	800–1000
ZrP(HT12 M-200-24)[c]	93.7	1000–1200
ZrP(HF1)[d]	83.5	1000–2000
ZrP(HF2)[d]	72.0	1000–3000
ZrP(HF3)[d]	53.5	1500–3500
ZrP(HF4)[d]	41.8	2000–4000

Taken from *New J. Chem.*, 2007, 31, 39–43; DOI: 10.1039/B604054C.

[a]Refluxing method: 3.0/6.0/9.0/12.0 M H_3PO_4 at 100°C for 24 h. ZrP([H_3PO_4]).

[b]Hydrothermal method: 3.0/6.0/9.0/12.0 M H_3PO_4 sealed into a Teflon®-lined pressure vessel and heated at 200°C for 5 h. ZrP(HT[H_3PO_4]-temperature-time(h)).

[c]Hydrothermal method: 3.0/6.0/9.0/12.0 M H_3PO_4 sealed into a Teflon-lined pressure vessel and heated at 200°C for 24 h. ZrP(HT[H_3PO_4]-temperature-time(h)).

[d]Hydrofluoric acid method: HF solution (5.0 M) at molar ratio of F^-/Zr^{4+} = 1, 2, 3 and 4 refluxed at 100°C for 24 h. ZrP(HF molar ratio of F^-/Zr^{4+}).

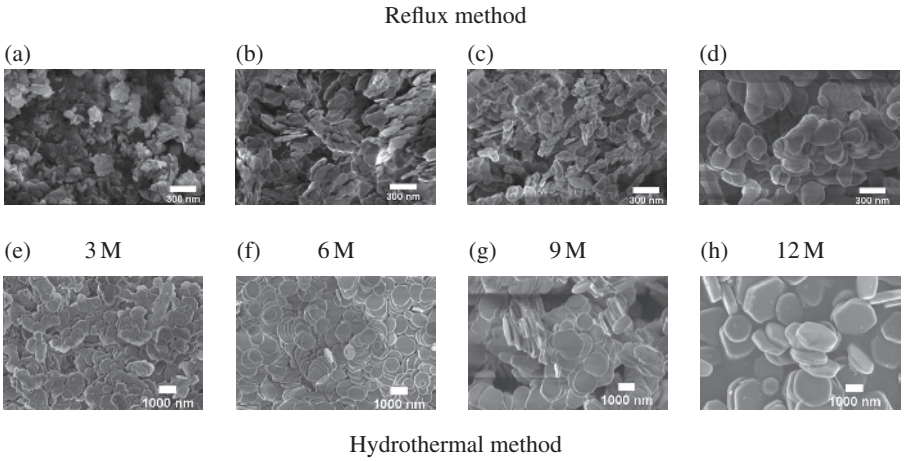

FIGURE 1.2 SEM images of α-ZrP particles prepared by refluxing the amorphous precipitated particles (top) and hydrothermally (bottom) for 24 h in increasing concentrations of H_3PO_4 (a and e) 3 M, (b and f) 6 M, (c and g) 9 M and (d and h) 12 M (Taken from: *New J. Chem.* 2007, *31*, 39–43; DOI: 10.1039/B604054C).

Camino Trobajo et al. observed a new phenomenon dealing with the synthesis of α-ZrP [9]. In their preparation of amorphous zirconium phosphate, they added a solution of zirconyl chloride in 2 M HCl to a solution of 1.25 M H_3PO_4 with constant stirring. The white solid that was obtained was washed with dilute phosphoric acid and dried in air. To their surprise, the X-ray pattern was that of crystalline α-ZrP. However, when they followed the method described by Clearfield and Stynes [3], they did obtain the amorphous solid. What Trobajo et al. found was that in their preparations there was always a significant amount of phosphoric acid present in the solid and this may have keyed the conversion to crystals. We shall return to this point again.

It is now necessary to describe several other features of the α-ZrP crystals that relate to their usefulness [10–12]:

1. The particles are ion exchangers in which cations readily replace the protons

$$Na^+ + Zr(HPO_4)_2 \cdot H_2O \leftrightarrows Zr(NaPO_4)(HPO_4) \cdot xH_2O + H^+$$

2. The layers can intercalate molecules by means of acid–base reactions

$$RNH_2 + Zr(HPO_4)_2 \cdot H_2O \leftrightarrows Zr(RNH_3PO_4)(HPO_4) \cdot xH_2O$$

3. Solid–solid exchange [13–15]
4. $$Zr(HPO_4)_2 \cdot H_2O + 2/z\ MCl_z \xrightarrow[1\,h]{100^\circ C} Zr(M_{2/x})(PO_4)_2 + 2HCl\uparrow + H_2O$$

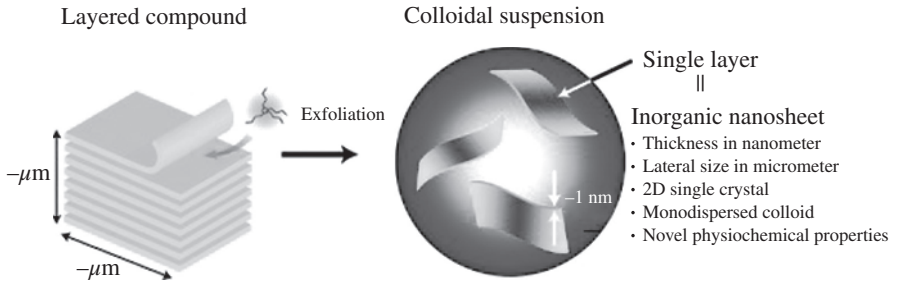

FIGURE 1.3 Schematic model illustrating the exfoliation of a layered compound into colloidal nano-sheets (Taken from: *Adv. Mater.* 2010, *22*, 5082–5104; DOI: 10.1002/adma.201001722).

5. The driving force here is the removal of HCl at elevated temperature. For example,

$$2\mathrm{LiCl} + \mathrm{Zr}\left(\mathrm{HPO_4}\right)\cdot \mathrm{H_2O} \xrightarrow[1\ \mathrm{h}]{100^{\circ}\mathrm{C}} \mathrm{Zr}\left(\mathrm{LiPO_4}\right) + 2\mathrm{HCl}\uparrow + \mathrm{H_2O}$$

The reverse reaction is also easily done, for example, treatment of the metal zirconium phosphate with gaseous HCl at 120°C. Similar reactions have been carried out with zeolites [16]. A summary of intercalation reactions of α-ZrP has been published [17]. Shortly after this publication, Mallouk et al. [11] examined the intercalation/exfoliation reactions of α-ZrP by use of atomic force microscopy (AFM) and transition electron microscopy (TEM). They utilized tetra(*n*-butyl)ammonium hydroxide (TBA^+OH^-) as the exfoliant (Figure 1.3). The rate-determining step was found to be the opening of the interlamellar space increasing this space. Then rapid diffusion of TBA^+ ions into the galleries occurs. A hydrolysis reaction occurs around the edges forming 4 nm hydrated zirconia particles around the layer edges. This reaction introduces phosphate ion into the solution and creates an equilibrium state. The hydrolysis may be suppressed by operating at 0°C.

Another way to exfoliate the layers is to titrate the crystals with propylamine [18, 19], using only one mole of amine per mole of α-ZrP. The process is slow enough that the amines arrange themselves at every other P–OH group. This places the propylammonium ions 10.6 Å apart and moves the layers so that the interlayer distance is more than 10 Å. Water can now flood the interlayer space and exfoliate the layers. Smaller amines also exfoliate the layers, but butylamine does not. Rather, it forms a series of phases as the amount intercalated increases. That is the case for amines with larger alkyl chains [20].

1.3 ZIRCONIUM PHOSPHATE-BASED DIALYSIS PROCESS

Given all these attributes of the crystalline particles, it is interesting that the first commercial application was for the amorphous ZrP. A group at the NIH wished to design a portable kidney dialysis system. People who suffer from renal problems

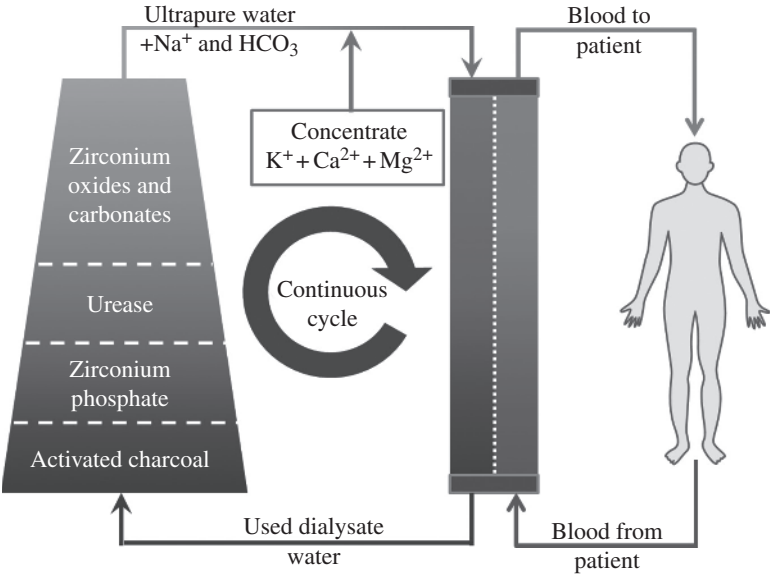

FIGURE 1.4 Schematic representation of the dialysis process.

need to undergo dialysis to remove all the toxins that accumulate in their system. This requires the use of an artificial kidney membrane with a flow of water across the membrane to wash the toxins down the drain. Being hooked up to this apparatus for several hours with a loud pump powering 100–250 gallons of water across the membrane was not an event to look forward to, as well as waiting for a room to become available and turning yellow while sitting in the hospital waiting room.

In the portable unit, the wash water would have to be recycled so sorbents were required. It turned out that activated charcoal could remove all of the toxins except urea. To remove the urea, after testing many sorbents, they fixed on putting the enzyme urease on amorphous zirconium phosphate. The urea was converted to NH_4CO_3 that then reacted with ZrP as in

$$\left(NH_4\right)_2 CO_3 + Zr\left(HPO_4\right)_2 \cdot nH_2O \rightarrow Zr\left(NH_4PO_4\right)_2 \cdot nH_2O + CO_2 + H_2O$$

In this process, it is necessary that the dialysate be slightly basic. This results in some hydrolysis of the zirconium phosphate accompanied by release of a small amount phosphate that is prevented from entering the dialysate by sorption with a layer of hydrous zirconia placed below the layer of ZrP (Figure 1.4). With purchase of this unit, the process of dialysis could be carried out in your own dwelling administered by a trained family member. All the systems were miniaturized so that the unit weighed about 60 lbs and operated quietly and with temperature control for the patients' comfort. Many hospitals use these units rather than the older method [21].

1.4 ZrP TITRATION CURVES

You might wonder why the amorphous ZrP rather than the crystalline form was used and that gives me a chance to describe this ZrP system in more detail. If we examine the titration curves (NaOH/NaCl) of the amorphous and crystalline samples shown in Figure 1.5, the curves are entirely different [22]. Note that with each increase in the addition of sodium ion, the pH increases for the gel. This is similar to polymer type ion exchangers where the Na^+ is distributed equally throughout the solid. In contrast, it turns out that with the fully crystalline solid, the sodium ion enters from the edges [10] and immediately forms a new phase, $Zr(O_3PONa)(O_3POH)\cdot 5H_2O$. This means that there are two solid phases within the same crystal. The phase rule can explain this behaviour:

$$f = C - P + 2$$

where f = the degrees of freedom, C = number of components and P = the number of phases. In ion exchange with the crystalline phase, there are two solid phases and the solution phase, the components are also three, one choice being the sodium ion concentration of the solid phase and of the solution phase and the solution hydrogen ion concentration. Since the pressure and temperature are constant, f = O. As a result, the exchange, in contrast to the gel, takes place at constant pH and constant sodium ion concentration (Figure 1.5) [22]. Thus, all sodium ion added at constant pH is taken up by the solid particles, and the reaction is

$$Zr\left(O_3POH\right)_2\cdot H_2O + Na^+ + 4H_2O \rightarrow Zr\left(O_3PONa\right)\left(O_3POH\right)\cdot 5H_2O$$

When all the α-ZrP is converted to the half sodium ion phase, the pH rises to that of the new phase and a second reaction at a new constant pH takes place:

$$Zr\left(O_3PONa\right)\left(O_3POH\right)\cdot 5H_2O + Na^+ \rightarrow Zr\left(O_3PONa\right)_2\cdot 3H_2O + H^+ + 2H_2O$$

The liberated H^+ is neutralized by the base from NaOH addition. The interlayer spacing for the half Na^+ ion phase is 11.8 Å and for the fully exchanged phase 9.8 Å.

An interesting fact is that as the gel is treated to produce crystals, the crystallinity can be changed very slowly. This is illustrated in Figure 1.6. It is seen that the gel has no discernible X-ray pattern [23]. However, upon refluxing at 48 h in 0.5 M H_3PO_4 (0.5 : 48), several very broad peaks appear. This broadness of peaks is the result of the nanoscale of the particles and their disorder. Interestingly, the first peak at $2\theta \equiv 8°$ gives a d-spacing of 11.0 Å. This first peak is the 002 or interlayer spacing value. Notice that at a slightly higher concentration of acid (0.8 : 48), the 2θ gives the d-spacing value that is very close to 7.6 Å. The other unit cell dimensions also change very slowly until a pattern like that of the 12 : 48 (refluxing for 48 h in 12 M H_3PO_4) sample is attained.

As the ZrP particles increase in crystallinity, the shape of the titration curves changes as shown in Figure 1.7. What transpires is that the sodium ion no longer

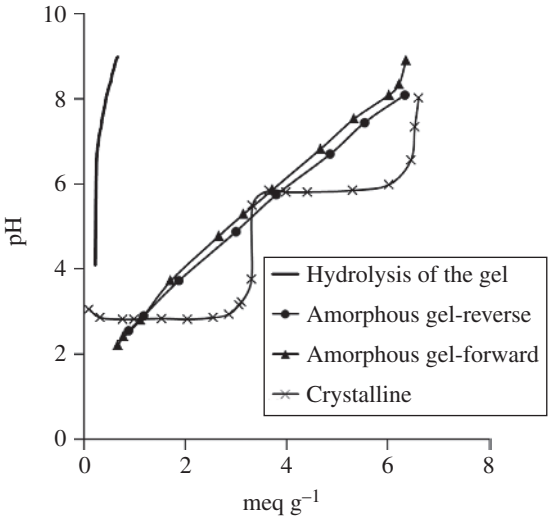

FIGURE 1.5 Potentiometric titration curve for α-ZrP. Titrant: 0.100 M (NaCl + NaOH); ×, highly crystalline sample; ▲, amorphous gel forward direction; ●, reverse direction. Solid line at far left is the extent of hydrolysis for the gel (Taken from: *Ind. Eng. Chem. Res.* 1995, *34*(8), 2865–2872; DOI: 10.1021/ie00047a040).

spreads throughout the particles but forms solid solution phases of different compositions of increasing Na^+ content [24]. Only when full crystallinity is achieved is the state of no degrees of freedom observed. The approximate sizes of the particles as obtained from X-ray peak broadening observed in the patterns in Figure 1.6 are given in Table 1.2 [23, 24]. Also, the ratio of phosphorus to zirconium for 0.5 : 48 was 1.934 and for 2.5 : 48, 1.959, as determined by chemical analysis. Only when the crystallinity is more than that of sample 12 : 48 is the P:Zr ratio 2, and even here, one needs to be careful that some hydrolysis has not occurred.

The very small particle size that we described in Table 1.2 was known to us early on as shown in Figure 1.2. The thickness of the 0.5 : 48 particles is 70 Å or 6 layers. Presumably, the non-refluxed particles are even smaller, especially in length. Under the conditions of rapid precipitation on mixing a soluble zirconium compound with H_3PO_4, the probability of achieving a perfectly regular layer and stacking these layers parallel to each other is small. The gel particles are of the order of 0.1 μm or even smaller [24]. One can imagine that the phosphate groups are tilted randomly away from their equilibrium positions in the crystals so that some P–OH groups point towards and others away from each other. This creates high electrostatic stresses near the layers but weak forces between the layers. Thus, water is sorbed as a means of reducing the coulombic forces through solvation. This is similar to the swelling exhibited by organic cation-exchange resins.

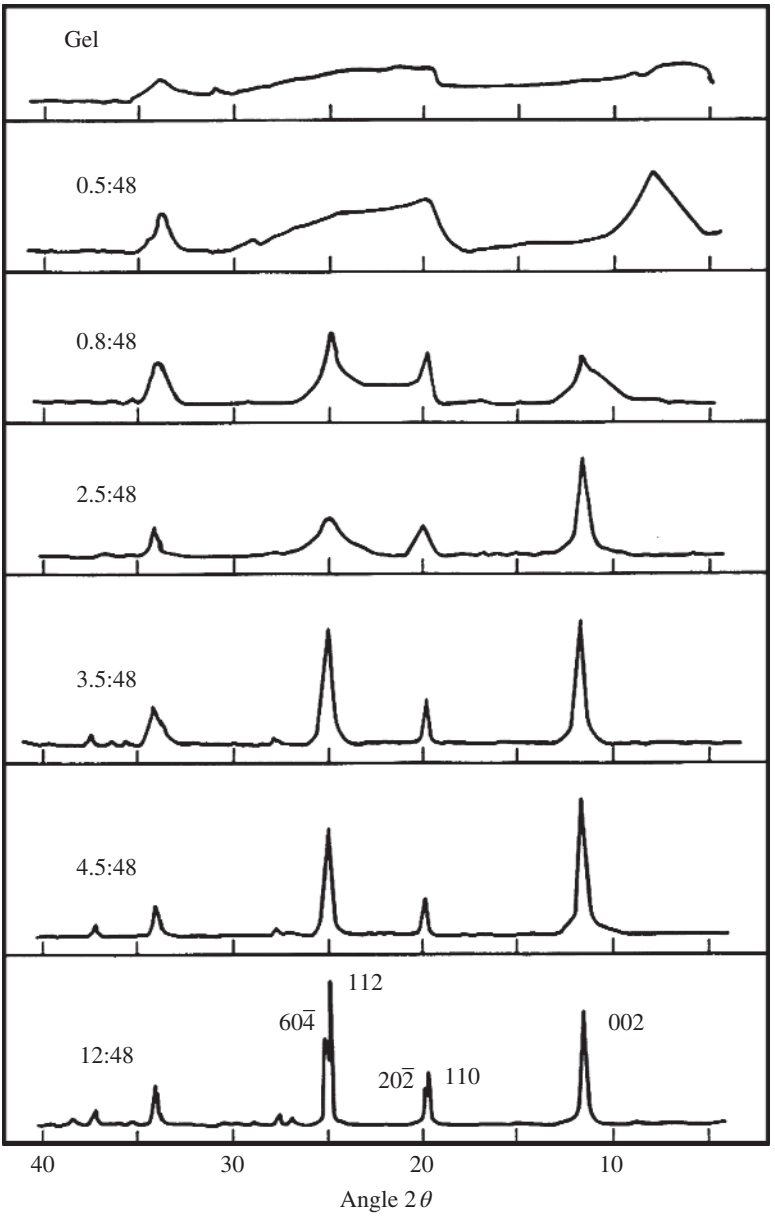

FIGURE 1.6 X-ray patterns of zirconium phosphates having different degrees of crystallinity. The numbers indicate the concentration of H_3PO_4 in which the gel was refluxed and the time of reflux in hours (Taken from: *Annu. Rev. Mater. Sci.* 1984, *14*, 205–229; DOI: 10.1146/annurev.ms.14.080184.001225).

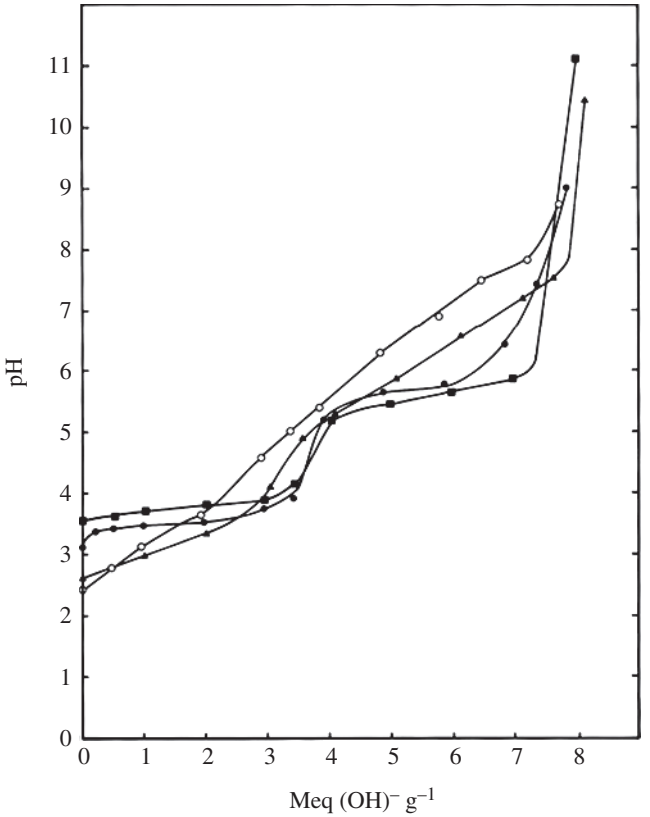

FIGURE 1.7 Titration curves for α-ZrP of low and intermediate crystallinities: 0.8:48 (○), 4.5:48 (●), 2.5:48 (▲), 12:48 (■). The numbers indicate the concentration of H_3PO_4 in which the gel was refluxed and the time of reflux in hours (Taken from: *Annu. Rev. Mater. Sci.* 1984, *14*, 205–229; DOI: 10.1146/annurev.ms.14.080184.001225).

TABLE 1.2 Crystallite sizes of zirconium phosphate gels

	d_{002}		Uncorrected d_{hkl}		Corrected d_{hkl}	
Sample[a]	Size (Å)	No. of layers	$d_{112,\,202}$	$d_{112,\,20\bar{4}}$	$d_{112,\,202}$	$d_{112,\,20\bar{4}}$
0.5 : 48	70	6				
0.8 : 58	100	13	210 (39)	260	300 (56)	360
2.5 : 48	330	44	250 (46)	100	350 (65)	140
3.5 : 48	330	44	550 (100)	360	770 (144)	510
4.5 : 48	400	53	770 (144)	550	1090 (200)	770

Taken from: *Ion Exchange and Membranes*, 1972, Vol. 1, 91–107.
[a]The numbers indicate the concentration of H_3PO_4 in which the gel was refluxed and the time of reflux in hours (i.e. 0.5 : 48 = 05 M H_3PO_4 refluxed for 48 h).

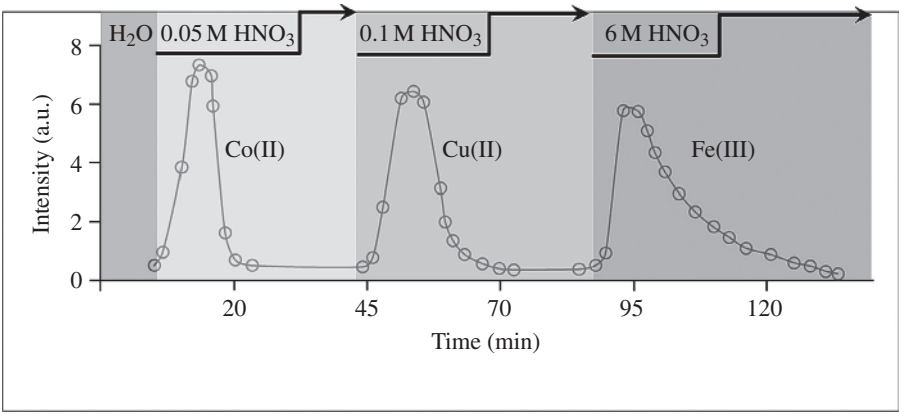

FIGURE 1.8 Chromatographic separation of three transition metal ions using the semi-amorphous ZrP 0.5 : 48 (Figure 1.6). The higher charge ion Fe (III) is more strongly held on the exchanger (Taken from: Clearfield, A., Jahangir, L.M. in Recent Developments in Separation Science, Navratil J. D. and Li, N. N. Eds, CRC Press, Boca Raton, FL. 1984 Vol. VIII. Ch. 4).

1.5 APPLICATIONS OF ION-EXCHANGE PROCESSES

In 1984, Clearfield and postdoc Jahangir published a paper titled 'New Tools for Separations' that listed 147 references [25]. It covered a wide range of topics including the differences in behaviour of the amorphous, semi-crystalline and crystalline forms of ZrP. Topics included separations of alkali metal ions, divalent and polyvalent cations, separation of lanthanides and actinides, nuclear waste processing and water purification. This paper also introduces θ-ZrP, a form of α-ZrP but containing 6 mol of water and an interlayer spacing of 10.4 Å. The amorphous gel phase was shown to behave as a weak field ion exchanger in the sense of Eisenman's theory [26]. The selectivity for the alkali cations is $Cs^+ > Rb^+ > K^+ > Na^+ > Li^+$ [27]. As the cation content increases, the selectivities change as predicted by Eisenman's theory to the strong field order that is just the reverse of the above order.

Selectivities of cations with higher charge are preferred by the amorphous (gel) ZrP, and some interesting separations of radioisotopes have been carried out using chromatographic separations. An example is given in Figure 1.8.

1.6 NUCLEAR ION SEPARATIONS

The amorphous zirconium phosphate was found to be active in the separation of radioactive ions because of its resistance to ionizing radiation, oxidizing media and strong acid solutions [28]. In general, it was found that separations for ions with the same charge were low, whereas those with different oxidation states were high [29, 30]. Fletcher Moore described a separation of Cm from Am by oxidizing americium to the plus five oxidation state where Cm does not oxidize. The Cm was then

preferentially solved by the amorphous ZrP, while Am(V) was only weakly sorbed [30]. Additional separations of actinides from lanthanides and actinides from each other were affected by the redox method [31, 32].

Subsequently, we developed a number of monophenyldiphosphonic acid phosphates of Zr^{4+} and Sn^{4+}. These compounds were found to be highly selective for ions of 3+ or 4+ charge but not for those of lower charge [33]. These ion exchangers are currently being utilized to develop separations of lanthanides from actinides and actinides from each other [34–36]. Such separations are required for the nuclear fuel cycle intended to recover fuel values from the reactor spent rods.

Interest in zirconium phosphate as an ion exchanger and sorbent in its many forms has existed to this day with about 30 papers a year on this subject. We provide only few examples.

Because of the versatility of the zirconium and titanium phosphates, new uses and novel forms are prepared to meet current needs. A composite titanium and zirconium phosphate cation exchanger was prepared by sol–gel mixing of polyaniline into precipitated ZrTi phosphate [37]. The best sample had an ion-exchange capacity of 4.52 meq g^{-1} with excellent chemical and thermal stability. It was found to remove heavy toxic metals, especially Pb(II) and Hg(II), from waste solutions.

Pb^{2+}, Zn^{2+}, Cd^{2+} and Ca^{2+} were exchanged by a nanoparticle, nearly amorphous sample, of α-ZrP [38]. The selectivity sequence is as in the order listed above. In a separate study, a similar ZrTi phosphate modified with Al^{3+} or Fe^{3+} was found to sorb uranium [39].

Studies have shown that hydrogen uranyl phosphate on *Serratia* sp. as a film showed 100% removal of ^{90}Sr, ^{137}Cs and ^{60}Co. However, the authors wished to use a non-toxic metal to replace the toxic U. Zr was found to fit the bill [40]. Zirconium in the form of glycerol 2-phosphate was immobilized as a biofilm onto polyurethane foam.

1.7 MAJOR USES OF α-ZrP

The list of uses and potential uses of α-ZrP is quite extensive, but among the most promising ones are ion exchanger, sensors, drug delivery, polymer composites, antimicrobials, fire retardants, non-soluble surfactants and catalysts. Some of them have been already mentioned, but not all of them will be described. For those described applications will be interspersed with additional properties of the α-ZrP particles both amorphous and crystalline.

1.8 POLYMER NANOCOMPOSITES

Polymer nanocomposites exhibit significantly enhanced physical and mechanical properties as opposed to conventional micrometre-scale inorganic filler-reinforced polymer composites [41]. Nanofillers have been based on TiO_2, $CaCO_3$, SiO_2 and clays, among others [42]. One difficulty encountered is incomplete dispersion of the nanofillers within the polymer. By exfoliating a montmorillonite clay and polymerizing nylon in the exfoliated media, a fairly uniform composite with the clay was obtained [43]. In general, clay-based composites exhibit enhanced modulus and gas

barrier properties of the polymer but also significant reduction in ductility and toughness [44]. Also, it is difficult to achieve very high purity, narrow particle size distribution and controlled aspect ratio of a clay. Many of the clay-based nanocomposites exhibit incomplete exfoliation of the clay, leading to inconsistent results.

Our original concern was to produce pure nanofillers of complete exfoliation so as to gain fundamental structure–property relationships. Our first effort involved the use of nanoparticles of α-ZrP with an epoxy polymer (diglycidyl ether of bisphenol A) [45]. A gel was formed in methyl ethyl ketone (MEK) by intercalating Jeffamine M 715 [$CH_3(CH_2CH_2O)_{14}CH_2CH_2NH_2$] between the α-ZrP layers. The X-ray powder pattern, shown in Figure 1.9 (top left), consists of a successive order of 00l peaks. The MEK was removed and the gel (5.2 wt%) was combined with the epoxy and a curing agent. Polymerization was carried out at 130°C. The resultant composite in Figure 1.9 indicates a uniform distribution of the ZrP throughout the polymer. The tensile module increased by 50%, and the yield strength improved by 10%. However, the ductility (elongation at break) was drastically reduced. The effect of incorporating the Jeffamines on the physical properties was not determined.

In a subsequent study, a 1 and 2% (vol%) α-ZrP dispersion in the epoxide was examined, and detailed facture toughness values are found to be similar to that of the neat epoxy [46]. There was no sign of crack deflection. Rather, the nano-platelets are broken into two halves as the crack propagated through them, a sign of strong bonding to the epoxy.

The effect of nano-platelets on the rheological behaviour of epoxy monomers with variations in nano-platelet exfoliation level of aspect ratio was investigated [47]. The results show that the presence of exfoliated nano-platelets in epoxy can significantly influence viscosity and lead to shear-thinning phenomena, especially when the aspect ratio of the nano-platelets is high. The Krieger–Dougherty model was employed to describe quantitatively the effectiveness of the nano-platelets upon the resultant rheological behaviour of the composites [48].

Studies on the effect of aspect ratios [49] and surface functionalization [50] by employing a combination of a long-chain alkylamine and a short-chain bulky amine were investigated. Gels of α-ZrP were prepared by treatment of α-ZrP particles

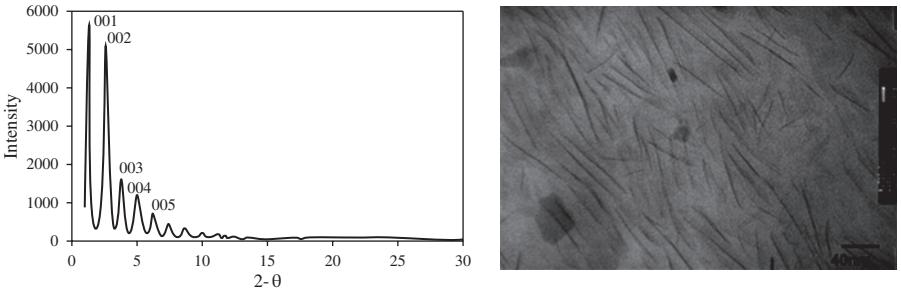

FIGURE 1.9 X-ray powder pattern of α-ZrP intercalated with Jeffamine M715 (left). The layered character of the compound is observed. The interlayer spacing is 73.27 Å. TEM image of M715-α-ZrP/epoxy showing high magnification of uniform dispersion and exfoliation of α-ZrP layers (right) (Taken from: *Chem. Mater.* 2004, *16*, 242–249; DOI: 10.1021/cm030441s).

(25–80 nm) with propylamine and mixed with polystyrene in a water-soluble organic solvent [51]. Hung et al. used melt compounding to incorporate ZrP into a styrene–butadiene polymer [52]. It was shown how the physics and chemistry incompatibility of the filler and polymer can be overcome.

Nanocomposites of poly(ethylene terephthalate) and α-ZrP or zirconium phenylphosphonate (ZrPPh) were prepared by melt extrusion [53]. Two and five weight percent composites were prepared in a twin-screw extruder and samples obtained by injection moulding. Many polymer composites have been prepared using ZrP or its derivatives aimed towards better fire retardancy or as proton conductors for fuel cells. These composites will be described later in connection with fuel cells. For our final effort, we attempted a nanocomposite for polypropylene (PP).

Preparation of PP nanocomposites appears to be most challenging. The low compatibility between PP and inorganic nano-platelets leads to poor dispersion and adhesion of nano-platelets in the PP mix, resulting in the low performance of the nanocomposites. However, because of the significant commercial importance of PP, improvement in the thermal stability and mechanical strength would dramatically enhance the utilization of PP in several engineering applications. The problem is the poor compatibility between the nanoparticle and the PP. Many efforts have been attempted to alter the nanoparticle, the PP or both to achieve compatibility [54–60].

Our own effort at compatibility was to prepare a mixed derivative, $Zr(O_3POH)_{2-x}(O_3P–CH_3)_x$ as shown in Figure 1.10, with $x = 0.66$, 1.0, 1.33 [54]. The X-ray patterns showed interlayer spacings of 8.4, 8.6 and 8.8 Å (7.6 Å for α-ZrP), respectively, for the three samples. The methyl groups impart a measure of hydrophobicity to the particles, and when sonicated in toluene, the 8.4 Å sample swelled to 9.4 Å. The reactions were carried out in cold toluene. Sonication was continued to the point (6 h) where very little of the nanoparticles precipitated. Gaseous propylene was dissolved in the toluene and an Figure 1.10 Schematic of reaction for the synthesis of α- ZrP and its methyl/

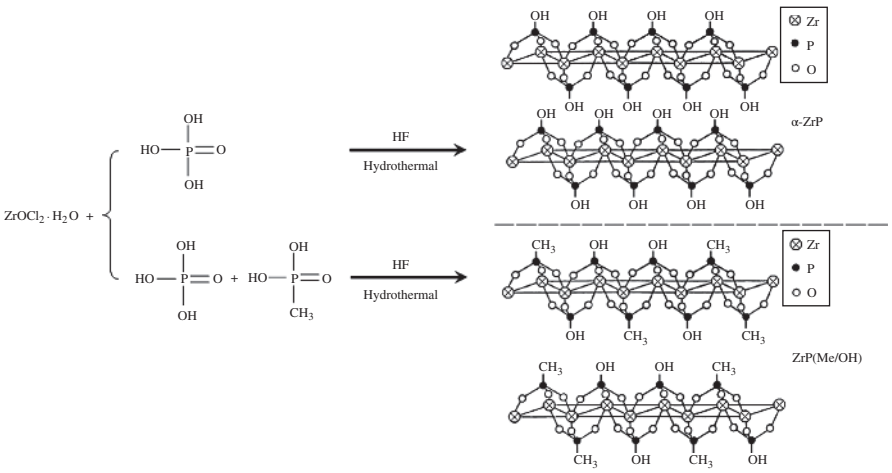

FIGURE 1.10 (Continued)

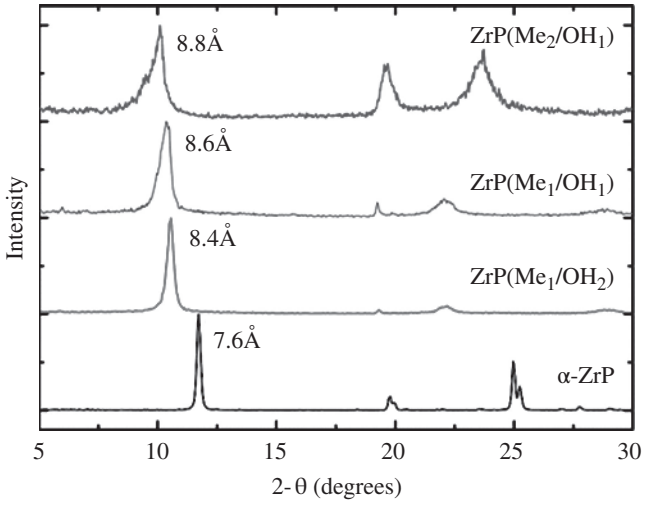

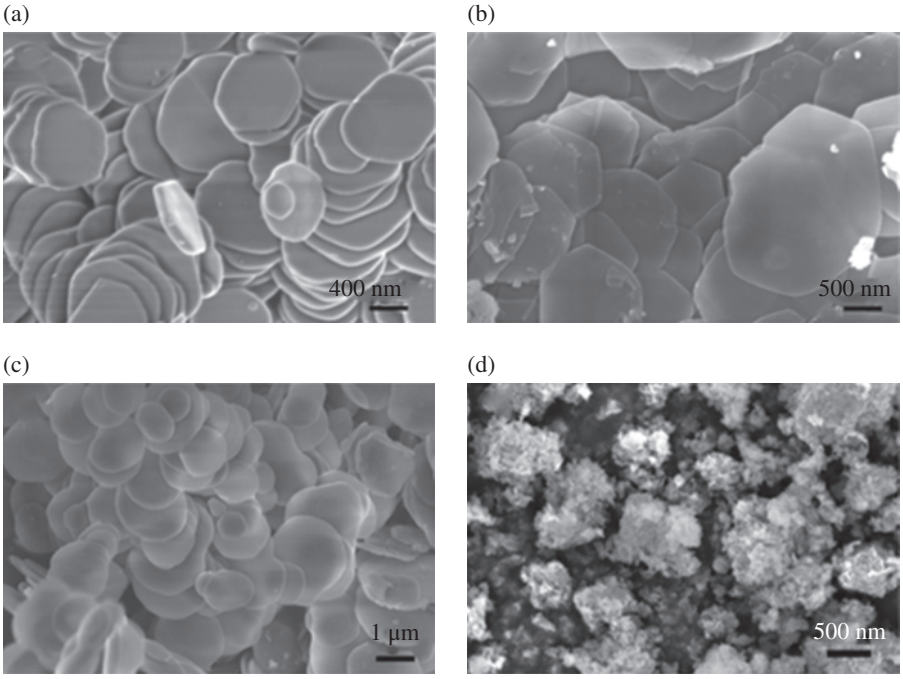

FIGURE 1.10 Schematic of the reaction for the synthesis of α-ZrP and its methyl/hydroxyl mixed derivative. At the bottom is the XRD (left) and SEM image (right) of (a) α-ZrP and its methyl/hydroxyl mixed derivatives: (b) $ZrP(Me_1/OH_2)$, (c) $ZrP(Me_1/OH_1)$ and (d) $ZrP(Me_2/OH_1)$ (Taken from: *Chem. Mater*. 2009, 21, 1154–1161; DOI: 10.1021/cm803024e).

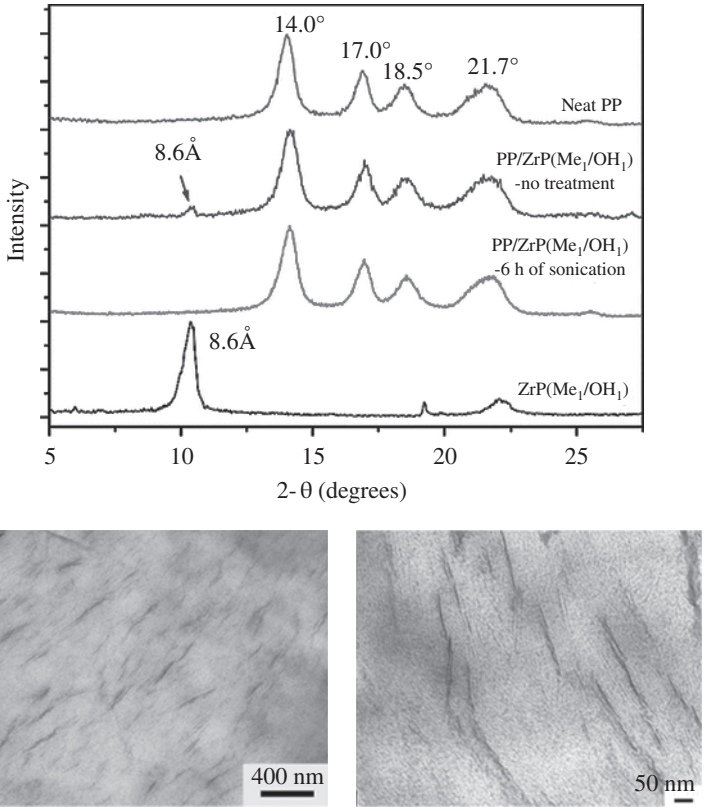

FIGURE 1.11 XRD pattern of PP/ZrP(Me_1/OH_1) nanocomposites (top). TEM images (bottom) of PP/ZrP(Me_1/OH_2) nanocomposite prepared with ultrasonicated ZrP(Me_1/OH_2) (Taken from: *Chem. Mater.* 2009, *21*, 1154–1161; DOI: 10.1021/cm803024e).

hydroxyl mixed derivatives, above, and the XRD and SEM images of the mixed derivatives (page 15) as (a) α- ZrP, (b) ZrP (Me_1,/OH_2); (c) ZrP(Me_1/OH_1); (d) ZrP (Me_2/OH_1). (Taken from Chem. Mater. 2009, 21, 1154–1161). organometallic catalyst added. To stop the reaction, 10% HCl was added. The PP was of the isotactic structure. The dispersion of the particles is fairly uniform as shown in Figure 1.11. However, complete exfoliation did not occur. The layers are grouped in stacks of two to five layers. It was reasoned that better compatibility would require a somewhat longer carbon chain balanced with better exfoliation character.

What the industry really desires is to be able to add the nanoparticles when the polypropylene is fluid at elevated temperature. In this way, they would not have to change their synthesis procedures. However, that is a daunting task. More recent work has concentrated on different approaches to achieve good composites.

Hung et al. claim that they were able to add α-ZrP nanoparticles to a styrene–butadiene copolymer during melt compounding [52]. Composites of polystyrene and polyethylene-vinyl acetate were prepared with organically modified α-ZrP, that is,

alkyl chains attached to the phosphonate head [61]. They used melt blending as a means of dispersing the particles into the polymer. A styrene–butadiene rubber was combined with α-ZrP that was modified with intercalated alkylamines of different chain lengths used to move the layers apart. The intercalation mechanism is described in some detail [62]. Casciola et al. [63] used dodecyl groups bonded to α-ZrP to prepare polymer composites with molten polyethylene. A number of starch polymer–α-ZrP composites were also prepared [64]. Many polymer composites are either prepared for flame retardation [61] or proton conduction that will be discussed in another section.

There is a need by the packaging industry to have wrapping materials and plastic bottles that prevent diffusion of O_2 through the package. The use of clays and other inorganic materials has been somewhat successful but not adopted.

1.9 MORE DETAILS ON α-ZrP: SURFACE FUNCTIONALIZATION

At this juncture, it is necessary to describe additional properties of the ZrP particles. It is now well known that silanes will bond to silica and to silicon to form self-assembled monolayers [65]. Since then, a veritable cornucopia of SAMs have been produced on these surfaces [66–73]. In addition, the SAMs may be functionalized by surface reactions or by prefunctionalization prior to preparing the SAM [71, 72]. As a result, a wide range of applications for SAMs have emerged. The functionalization of surfaces allows the worker to change the surface properties such as friction, wettability, adhesion, and so on. Furthermore, the end groups of the silanol may be changed in an almost unlimited number of ways for applications as chemical sensors and biosensors; in microelectronics, thin film technology and cell adhesion photolithography; and in a variety of important protective coatings, composites and catalytic materials [67, 72].

A schematic representation of the surface of α-ZrP is shown in Figure 1.1(b). The surface is just a slice of one of the layers and therefore should react with a number of ligands. We have recently shown that the surface indeed does bond with silanes, epoxides, isocyanates and acrylates directly. The silanes are suspended in hot toluene and allowed to react with dewatered α-ZrP [74]. In addition to these ligands, we have been able to bond polyethylene glycols (PEGs) to the surface in two ways. In the first, we used a carbodiimide [75], *N*,*N*′-diisopropylcarbodiimide, to activate the surface as depicted in Figure 1.12. The other technique is to add Zr^{4+} or Sn^{4+} to the α-ZrP in water. These ions replace the protons on the surface, producing an arrangement similar to the arrangement of the metal ions within the layers

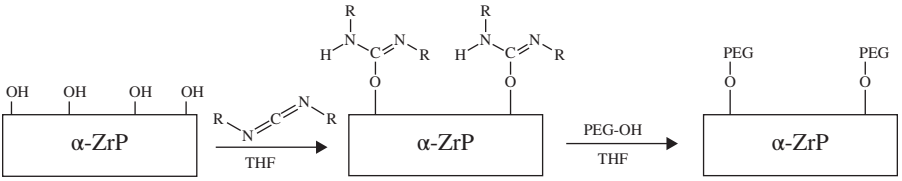

FIGURE 1.12 Reaction scheme for the surface modification via phosphate activation by a carbodiimide.

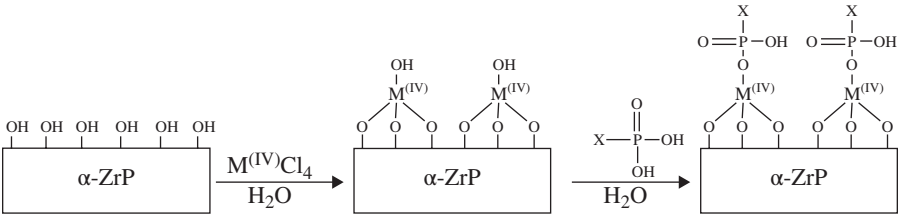

FIGURE 1.13 Reaction scheme for the surface modification using tetravalent metals to coordinate to the phosphate groups on the surface of ZrP, followed by the addition of a phosphonic acid to complete the coordination.

(Figure 1.13). As a result, any phosphate or phosphonic acid can be affixed to the metal ion surface. PEGs can readily be converted to a phosphate by oxidation of the alcohol group with $POCl_3$. In fact, a whole variety of alcohols may be oxidized and bonded to the surface metal ions. A pictorial summary of the surface functionalized in this manner is provided in Figure 1.13 and the totality of reactions in Figure 1.14. The ability to carry out these functionalizations opens up vast new possibilities that will be described in what follows.

1.10 JANUS PARTICLES

Janus particles were named after the Roman God of doors by Nobel Laureate Pierre-Gilles de Gennes [76]. These compounds have two halves that differ in chemical properties. An example is a layered compound that has one ligand on the topside and a different ligand on the underside. There are many ways of preparing Janus particles such as layer-by-layer self-assembly or in general shielding part of the particle while coating the unshielded part (Figure 1.15) [77–81]. While many uses are proposed for these materials, the problem is the lack of methods to prepare them in quantity [80, 81]. Amphiphilic Janus particles absorb to interfaces and foam surfaces [82, 83]. Janus particles can play a role in catalysis [84] and applications in display technology, switching between dark and light sides using magnetic or electric fields [85].

Our synthesis of Janus particles involved reaction of the α-ZrP nanoparticles with octadecylisocyanate to cover both outer surfaces [86]. The particles are then exfoliated and separated using foams or water–oil mixtures (Figure 1.16).

Janus particles are strongly adsorbed onto interfaces, where they act as surfactants. Our amphiphilic α-ZrP nano-sheets have a large aspect ratio due to their very small layer thickness as shown earlier by Alberti et al. [19]. Their large lateral surface area offers strong adsorption energy at the oil–water interface. An oil-in-water emulsion stabilized by the α-ZrP Janus particles as surfactant was prepared at room temperature by sonication. This emulsion was stable for months, whereas an emulsion prepared from only α-ZrP particles was stable for only a few hours [86].

These initial experiments are very promising. Given the fact that the size of the ZrP particles can be controlled and there is a large choice of what is put on the surface, the

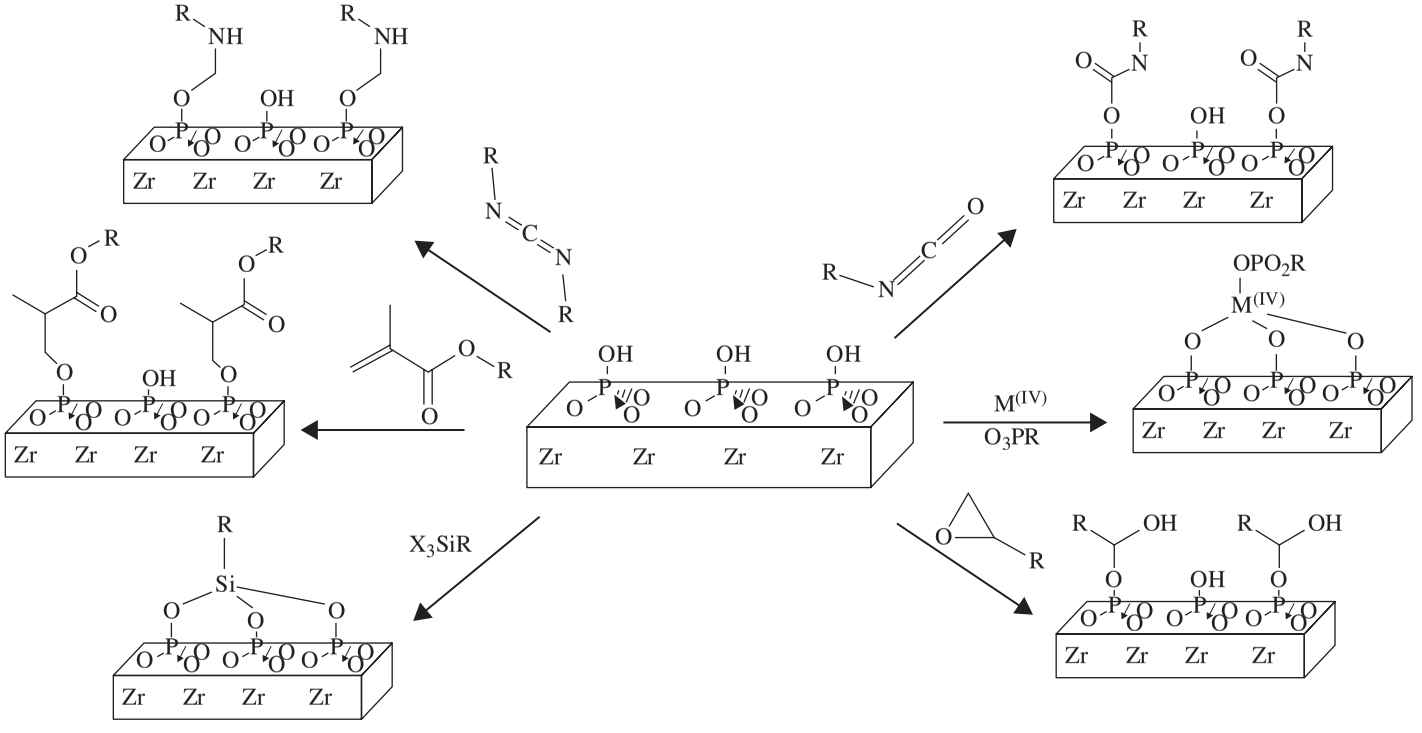

FIGURE 1.14 The many ways that the surface of α-ZrP may be functionalized.

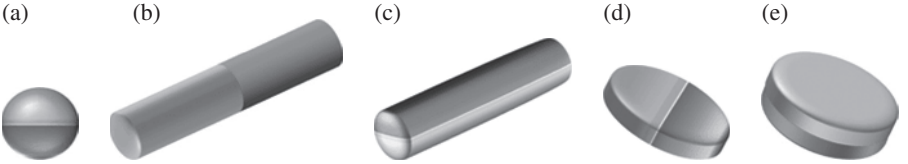

FIGURE 1.15 Schematic representation of the possible Janus particle architectures: (a) sphere, (b and c) cylinders and (d and e) discs. The light and dark portions differ in hydrophobic/hydrophilic character (Taken from: *Soft Matter* 2008, *4*, 663–668.

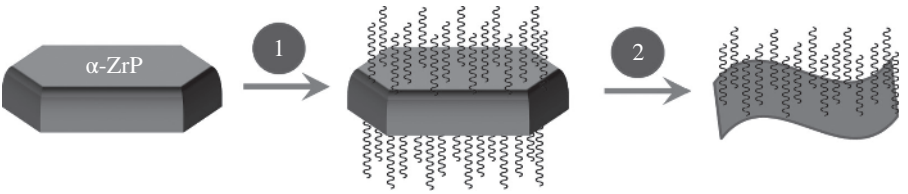

FIGURE 1.16 Schematic representation of the fabrication of surface-modified amphiphilic nano-sheets. The initial step (1) consists of grafting a coupling agent over the surface of α-ZrP. Subsequently, the exfoliation of the crystals is carried out (2) to obtain the surface-modified amphiphilic nano-sheets.

Janus particles can be tailored for many applications. To increase the percentage of Janus particles in each preparation, it is necessary to decrease the number of layers per particle, and we are now studying how this may be accomplished.

1.11 CATALYSIS

α-ZrP has a long history of use as a catalyst. It is mildly acidic and can be altered by surface area expansion, by intercalating metal ions, by formation of porous types and by intercalation of catalytically active molecules. Presumably, the first catalytic reaction using α-ZrP was between Cu^{2+}-exchanged α-ZrP and carbon monoxide [87]. High levels of oxidation were obtained with O_2 at 250–300°C. Subsequently, it was determined that the Cu^{2+} could easily be reduced to Cu metal by H_2 at 150°C [88]. The copper metal was deposited around the sides and top and bottom of the ZrP crystals, while H^+ replaced the Cu^{2+}. Interestingly, on standing in air at room temperature, the copper metal oxidized back to Cu^{2+} and diffused back into the ZrP layers. Presumably, the reaction is as shown in the equation, but no attempt to isolate H_2O_2 was made:

$$Cu^{\circ} + Zr\left(O_3POH\right)_2 \xrightarrow[RT]{O_2} ZrCu^{2+}\left(PO_4\right)_2 + H_2O_2$$

By 1980, reactions in which ZrP was used as a catalyst included dehydrogenation, isomerization, polymerization and alkylation [89]. The oxidative dehydrogenation of cyclohexene to benzene was effected with $ZrCu(PO_4)_2$. Complete oxidation to CO_2

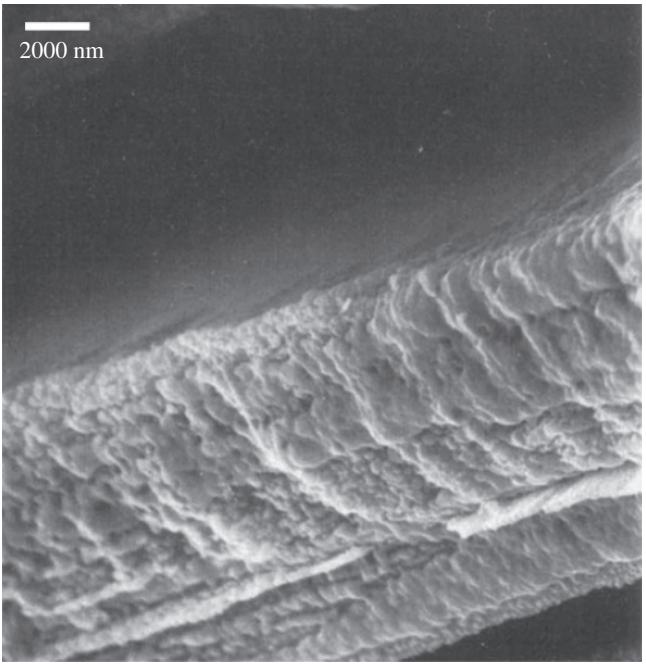

FIGURE 1.17 SEM image of silver particles on the surface of ZrP particles, grown by the reduction of silver ions previously loaded into the layers of α-ZrP (Taken from: *J. Chem. Soc. Faraday Trans.* 1984, *80*, 1579).

and H_2O could also be achieved [90, 91]. We also were able to prepare nanometre-sized clusters of Cu by limiting the amount of copper ion exchanged into the α-ZrP layers. Ag^+ was also reduced to Ag° with H_2 at temperatures as low as 60°C and also showed reversible behaviour (Figure 1.17) [92]. A good summary of our early work is available [93]. This paper discusses the acidity of ZrP surfaces and reactions such as dehydration of alcohols to olefins, polymerization of olefins, oxidation reactions with transition elements between the layers, hydrogenation reactions, oxidative dehydrogenation and other reactions.

Costantino et al. carried out base catalysis using the Michael reaction as an example [94]. To increase the surface area of the catalyst, they exfoliated the layers with propylamine titration and then removed the amine with HCl under sonication. This procedure increased the surface area from 0.5 to 17 $m^2\ g^{-1}$. A number of reactions with 85–98% yields using the Na^+ form of α-ZrP were recorded, for example, as given below:

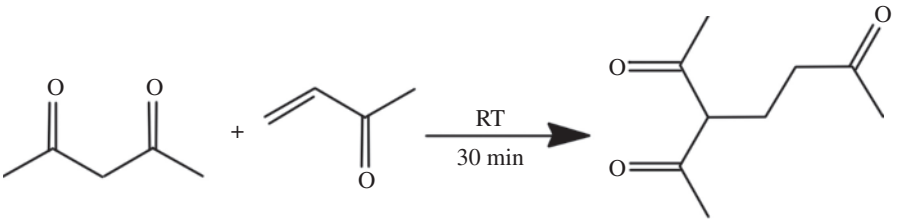

Almost all catalytic reactions with α-ZrP are now carried out with high-surface-area materials. One method involves separate nucleation and ageing steps (SNAS) [95]. The ZrP particles were prepared in a colloid mill, refluxed in 15 M H_3PO_4 and then spray-dried to form microspheres with a diameter of 5–45 μm. These spheres were then used to convert fatty acid methyl esters to monoethanolamines. The fatty acids are high cost and need to produce high-cost products [96]. Fatty acid derivatives combined with amino alcohols, through acylations, can produce high-cost amides that are used in pharmaceutical and surfactant products. These microspheres were shown to effect the reactions in high yield under mild conditions. Other catalytic reactions to note are the intercalation of Cu(Salen) into α-ZrP to oxidize cyclohexene with dry tert-butyl hydroperoxides [97]. Olefin oxidation with dioxygen was catalysed by porphyrins and phthalocyanines intercalated into α-ZrP [98]. Alvaro and Johnstone prepared large-surface-area ZrP that could be highly loaded with Pd, Pt and Ni ions [99]. The ions were readily reduced to the metal state with H_2 at 400°C or with sodium tetrahydroborate at room temperature. These materials were very effective in the hydrogenation of alkenes.

The reader should be satisfied with these few examples to recognize the widespread use of α-ZrP as a catalyst and host for a variety of molecules, ions and metals to develop a useful search of the literature. A search of the literature from 2007 to 2013 yield 131 papers showing that the search for new catalysts based upon ZrP is an ongoing process.

1.12 CATALYSTS BASED ON SULPHONATED ZIRCONIUM PHENYLPHOSPHONATES

Another facet of the catalysis story is to recognize that there is a large literature on the preparation of zirconium and tin (IV) phenylphosphonates and their sulphonated forms. Therefore, it is necessary to begin with some facts about zirconium phenylphosphonate, $Zr(O_3PC_6H_5)_2$. This compound has a layered structure similar to that of α-ZrP. Heating at 140°C for 4 days produced the nanoparticles shown in Figure 1.18. Heating at 200°C hydrothermally for 30 days was necessary to obtain well enough formed crystals to determine the structure from X-ray powder data [100]. A view of the structure is shown in Figure 1.19. Because the phenyl rings are only 5.3 Å apart, the π–π overlap is strong and the layers resist interlayer expansion. However, by preparing mixed derivatives with H_3PO_4 to include phosphate groups (Figure 1.20), they can function as does α-ZrP. It was also advantageous to sulphonate the phenyl ring (Figure 1.21). The early history of preparing sulphonates of phenylphosphonate and phosphate derivatives is detailed in a recent book [101]. However, the catalytic behaviour of this molecule is of interest here.

Sulphonated or zirconium sulphophenyl phosphonate (ZrSPP) is a strong Brönsted acid and may be used in organic solvents permitting many catalytic reactions [102]. A series of papers using ZrSPP as catalyst were carried out by Curini et al. at the University of Perugia [103, 104]. The reactions they reported on include the preparation of cyclic and acyclic β-amino alcohols by addition of amines to epoxides [103], cyclic ketals and thioketals [104]. Early papers by

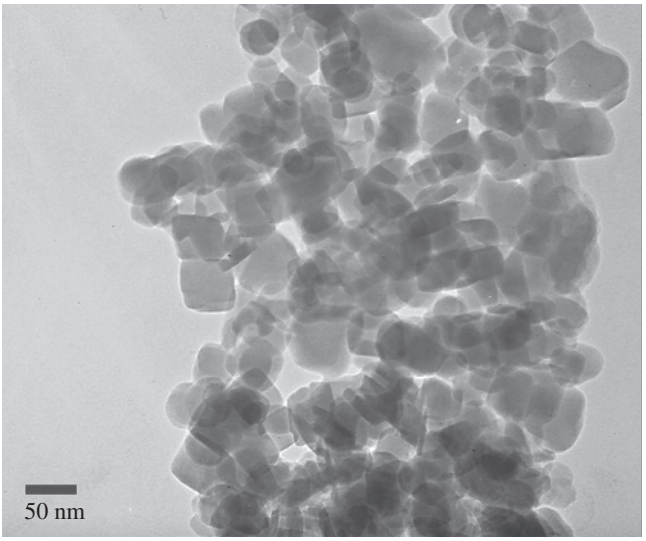

FIGURE 1.18 SEM image of zirconium phenylphosphonate particles grown hydrothermally at 140°C, 3 days, HF/Zr = 3 (Taken from: Clearfield, A. In *Environmental Applications of nanomaterials: Synthesis, Sorbents and Sensors*; Fryxell, G. E., Guozhong, C., Eds.; Imperial College Press, London, UK, 2007, p. 89).

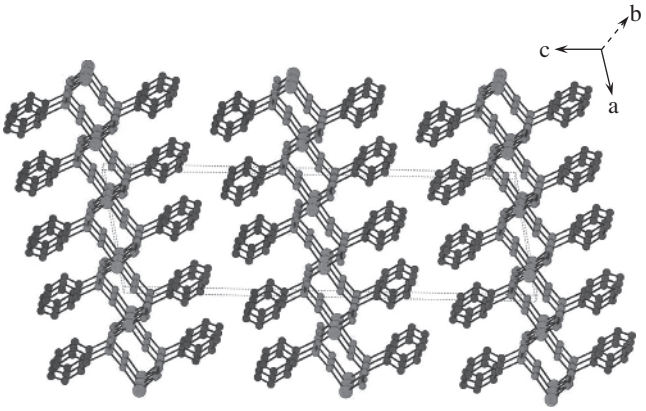

FIGURE 1.19 Schematic structure of zirconium phenylphosphonate as viewed down the *b*-axis direction (Taken from: Clearfield, A. In *Environmental Applications of nanomaterials: Synthesis, Sorbents, and Sensors*; Fryxell, G. E., Guozhong, C., Eds.; Imperial College Press: London, UK, 2007, p. 89).

the Curini group used a mixed ligand catalyst, $Zr(O_3PCH_3)_{1.2}(O_3PC_6H_4SO_3H)_{0.8}$ [105, 106]. It was found to be an efficient catalyst for the tetrahydropyranylation of alcohols and phenols. Additional related papers in use of such catalysts appeared regularly [107]. It was also shown that the mixed methane-sulphophenyl

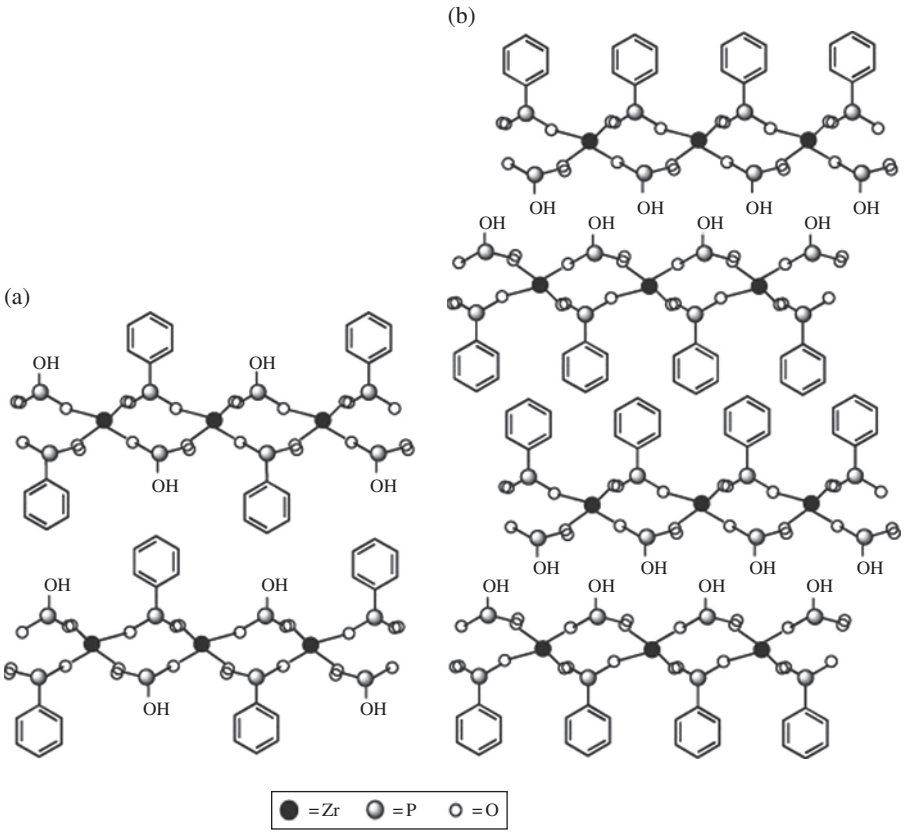

FIGURE 1.20 Schematic representation of two mixing patterns of zirconium phenylphosphonate phosphates. (A) Layers of mixed phenyl and phosphate groups (B) Staged structure with alternating layers of phenyl and phosphate groups. (Taken from: *Appl. Catal. A: Gen.* 2009, *353*, 236–242.

phosphonate mediated a regioselective synthesis of 2,3-disubstituted tetrahydro-2H-indazols. *In vivo* evaluation of these compounds proved the presence of anti-inflammatory activity without any gastric injury [108]. More recent work in China showed that the ZrSPP was an efficient and stable solid acid catalyst for the carbonylation of formaldehyde [109].

The next episode in catalysis results from our ability to functionalize the surface of the ZrP layers. In a separate set of α-ZrP nanoparticles, tris(2,2′bipyridyl) ruthenium(II), $Ru(bpy)_3^{2+}$, was intercalated into α-ZrP [74]. These intercalated particles were also surface functionalized with octadecyltrichlorosilane (OTS). The particles were highly hydrophobic as both surfaces contained the C_{18} silane. Two bottles were filled with a mixture of hexanes and water. To one is added the $Ru(bpy)_3^{2+}$/ZrP and to the other the surface-functionalized nanoparticles with $Ru(bpy)_3^{2+}$ between the layers. The hydrophilic particles reside solely in the water,

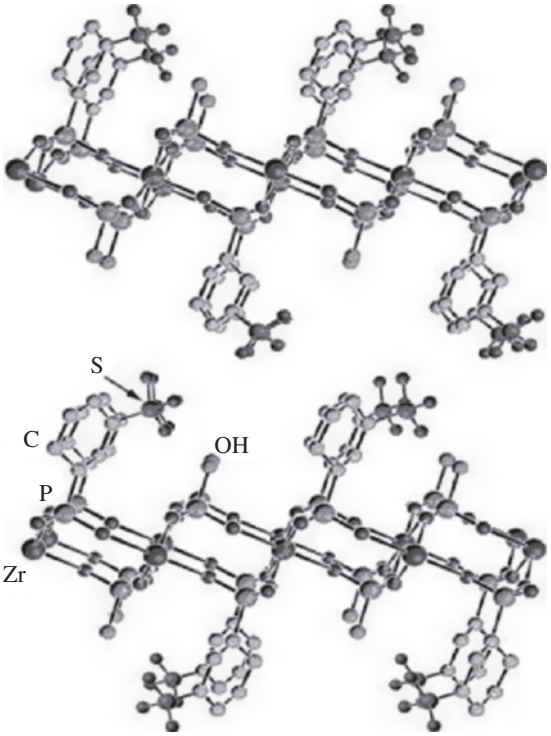

FIGURE 1.21 Schematic representation of zirconium phosphate sulphophenylenphosphonate (Taken from: *Solid State Ion*. 2005, *176*, 2893–2898; DOI: 10.1016/j.ssi.2005.09.042).

and the hydrophobic C_{18}-functionalized particles are all in the organic layer (Figure 1.22) [74].

The fact that the α-ZrP particles can be functionalized to the point where they can be dispersed in non-polar liquids indicates that they have a role to play in catalysis. An organometallic catalyst may be tethered to the support layer via flexible linkers. The dispersion of these nanoparticles in the fluid is as close as possible to being a homogeneous catalyst but with the advantage that the catalyst can be easily recovered and reused. The products would remain in the solvent and are recovered by conventional methods. Our first experiment involved the addition of Wilkinson's catalyst to propyl (diphenylphosphine) triethoxysilyl linker bonded to the surface of α-ZrP (Figure 1.23). 1-Dodecene was hydrogenated in toluene in very high yield. The reaction was repeated 15 times with no decrease in yield and no detectable catalyst in the toluene solvent.

In addition to its catalytic usage, ZrSPP is an excellent proton conductor. This fact requires that we pursue the applications to fuel cell technology.

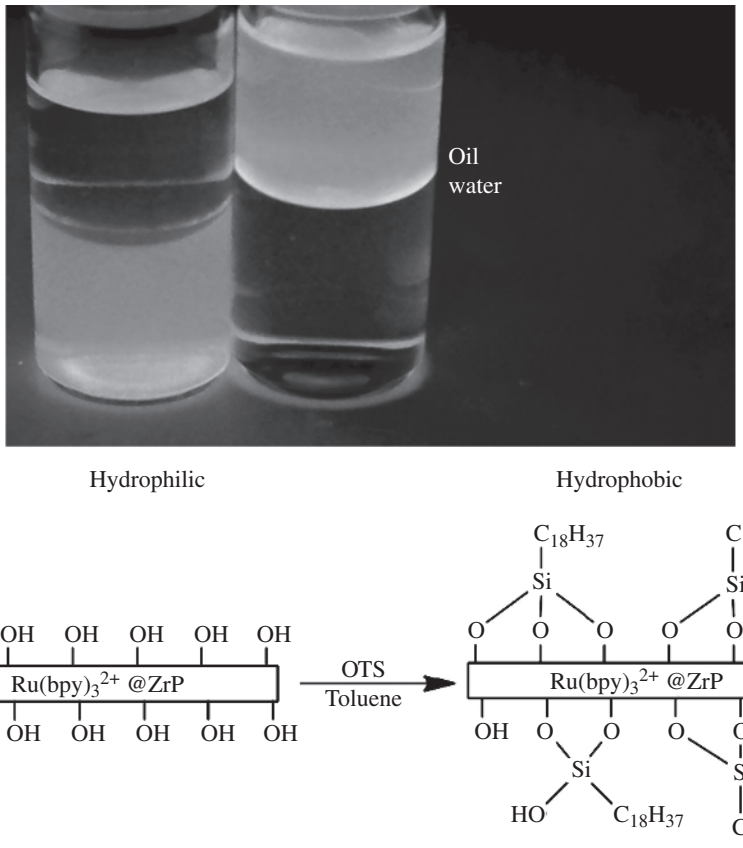

FIGURE 1.22 Zirconium phosphate, previously loaded with tris-(2,2′-bipyridine) ruthenium(II), surface modified with octadecyltrichlorosilane (OTS), making the nanoparticles compatible with non-polar solvent (Taken from: *Chem. Mater.* 2013, *25*, 723–728; DOI: 10.1021/cm303610v).

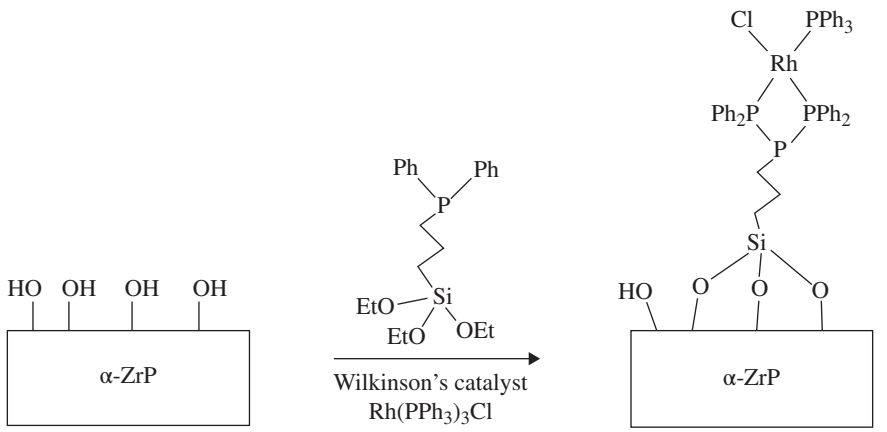

FIGURE 1.23 Scheme showing the addition of the silyl linker and catalyst on the surface of α-ZrP particles.

1.13 PROTON CONDUCTIVITY AND FUEL CELLS

α-ZrP is inherently a proton conductor. Early studies showed that the proton conductivity depends upon its crystallinity and the relative humidity [110, 111]. Table 1.3 summarizes the conductivity of α-ZrP of different crystallinites. The specific conductance decreases as the crystallinity increases. The explanation is that the surface area decreases in the same order and proton conduction is higher on the surface because of the higher surface water content and a lower order of confinement [112]. The protons in the bulk of the particles move slowly parallel to the layers to access the solution.

Subsequently, we prepared $Zr(O_3POH)_{1.1}(O_3PC_6H_4SO_3H)_{0.9}$, from the corresponding phenylphosphonate phosphate, in fuming sulphuric acid at 60°C [113]. Alberti et al. prepared a similar compound of composition $Zr(O_3C_6H_4SO_3H)_{0.73}(O_3PCH_2OH)_{1.27}$ [114]. This compound was shown to be a pure proton conductor. Arrhenius plots at several RH are shown in Figure 1.24. The highest conductivity at 295 K was 1.65×10^{-2} S cm^{-1}. Somewhat higher conductivities were obtained at 278 K for more highly sulphonated Zr and Ti compounds as shown in Table 1.4. The zirconium and titanium phenylphosphonates were sulphonated in fuming sulphuric acid and recovered by addition of methanol to the diluted acid followed by centrifugation [115]. More recently, chlorosulphonic acid was used in the preparation for better control of the reaction.

The titanium compound experiences a certain amount of cleavage of the P–C bond as the formula derived from elemental analysis and thermogravimetric analysis was $Ti(O_3POH)_{0.25}(O_3PC_6H_5)_{0.12}(O_3PC_6H_4SO_3H)_{1.63}\cdot 3.64H_2O$ as opposed to the fully sulphonated zirconium phosphonate, $Zr(O_3PC_6H_4SO_3)_2\cdot 3.6H_2O$. These sulphonated derivatives are among the best known proton conductors [115].

Before proceeding to discuss fuel cell electrodes, forgive me for pointing out a little investigated fact about the ZrSPP materials. They are excellent ion-exchange materials that arise from the ready displacement of the sulphonic acid protons. This is illustrated in Table 1.5 [116]. The increase in K_d values as a function of ion exchange and size allows for potential easy separations of these ions. We also note that the compound with the greater amount of sulphonic acid groups gave much

TABLE 1.3 Specific conductance of α-ZrP samples obtained by different methods of preparation and ordered according to their degree of crystallinity (T = 25°C)

Sample	Preparation method	Specific conductance (Ω^{-1} cm^{-1})
1	Precipitation at room temperature, amorphous	8.4×10^{-3}
2	Precipitation at room temperature, amorphous	3.5×10^{-3}
3	Refluxing method (7 : 48)[a], semi-crystalline	6.6×10^{-4}
4	Refluxing method (10 : 100), crystalline	9.4×10^{-5}
5	Refluxing method (12 : 500), crystalline	3.7×10^{-5}
6	Slow precipitation from HF solutions, crystalline	3.0×10^{-5}

[a]Numbers in parentheses indicate the concentration of H_3PO_4 in molarity and the number of hours refluxed, respectively.

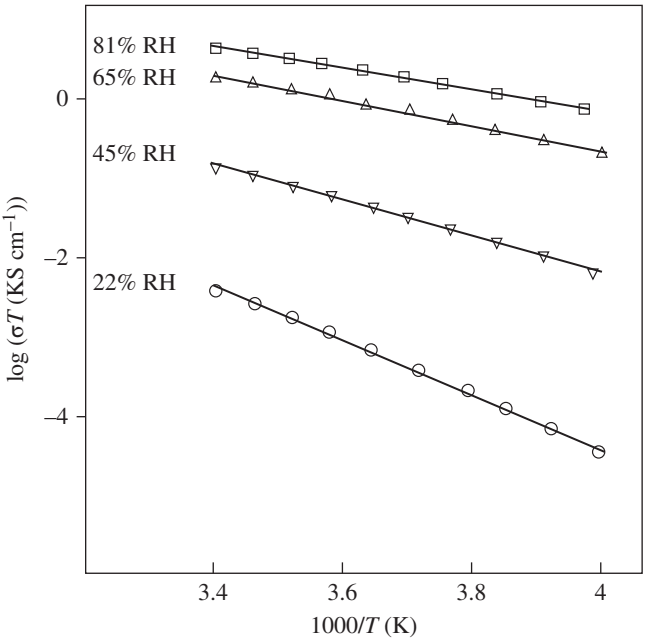

FIGURE 1.24 Arrhenius plots of log (σT) as a function of 1000/T for $Zr(O_3PC_6H_4SO_3H)_{0.73}(O_3PCH_2OH)_{1.27}$ at different relative humidities (Taken from: *Solid State Ionics* 1992, *50*, 315–322; DOI: 10.1016/0167-2738(92)90235-H).

TABLE 1.4 Conductivity in reciprocal Ω·cm at 5°C as a function of relative humidity for zirconium and titanium sulphophenylphosphonates

	Relative humidity (%)				
Sample	20 (3)[a]	30 (3)	50 (4)	65 (4)	85 (4)
EWS-3-89 (Zr)	5.0×10^{-6}	2.0×10^{-6}	1.1×10^{-3}	7.8×10^{-3}	2.1×10^{-2}
EWS-4-1 (Ti)	4.0×10^{-5}	3.0×10^{-3}	1.2×10^{-2}	7.2×10^{-2}	1.3×10^{-1}

[a]Number in parenthesis is the estimated error in the humidity measurement.

higher K_d values. A thermodynamic treatment of this ion-exchange behaviour is available [27, 117].

There is currently a great effort directed towards development of workable fuel cells because of their energy efficiency. Efficiencies as high as 70–80% are possible for fixed site units and 40–50% for transportation applications versus the current 20–35% with internal combustion engines [118]. For transportation purposes, proton-exchange membrane fuel cells (PEMFC) using H_2 as the fuel are preferred. A schematic drawing of such a fuel cell is given in Figure 1.25. The key ingredient in the PEMFC is the solid polymer membrane that conducts protons from the anode to the cathode. The most preferred membranes are fluorocarbon in nature to which are

TABLE 1.5 Distribution coefficient for alkali and alkaline earth metal ions on exchanger MY-IV-95, MY-VI-2 and amorphous zirconium phosphate for comparison

	K_d (ml g^{-1})		
Ion	MY-IV-95[a,b]	MY-VI-2[a,c]	Amorphous ZrP[a,d]
Li^+	110	—	7
Na^+	205	—	11
K^+	1,500	650	120
Cs^+	6,500	—	1600
Mg^{2+}	21,000	9,800	—
Ca^{2+}	8,9000	37,000	—
Ba^{2+}	400,000	190,000	—

[a] K_d at pH = 2.00 and a metal loading of 0.1 meq g^{-1}.
[b] $Zr(O_3PC_6H_4SO_3H)_{0.767}(O_3POH)_{1.23}$.
[c] $Zr(O_3PC_6H_4SO_3H)_{0.43}(O_3POH)_{1.57}$.
[d] Calculated from selectivity coefficient given in Ref. [27].

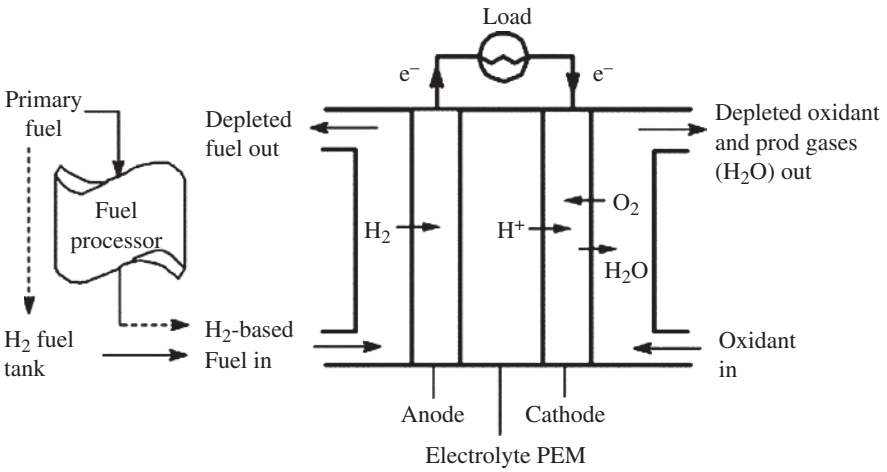

Anode (fuel) reaction: $H_2 = 2\,H^+ + 2\,e^-$

Cathode (oxidant) reaction: $1/2\,O_2 + 2\,H^+ + 2\,e^- = H_2O$

Total reaction: $H_2 + 1/2\,O_2 = H_2O$

FIGURE 1.25 Schematic representation of a proton-exchange membrane fuel cell (PEMFC) system using on-board or on-site fuel processor or on-board H_2 fuel tank (Taken from: *Catal. Today*, 2002, *77*, 17–49; DOI: 10.1016/S0920-5861(02)00231-6).

affixed sulphonic acid groups (Nasicon). These membranes are excellent electronic insulators with high proton conductivities of the order of 10^{-2} S cm^{-1} [or $(\Omega\ cm)^{-1}$]. The membranes require water as the main proton conduction medium and so work best at temperatures below 100°C. The problem arises from the fact that the H_2 must

be generated by an on-site fuel processor from methane or methanol. In the process, CO is also generated, which poisons the anode catalyst, platinum [119]. However, operation of the fuel cell at 120–130°C would eliminate this problem, but the membrane requires a considerable external pressure to avoid water loss [118, 119]. At temperatures of 140–160°C, direct methanol fuel cells (DMFC), where methanol is used directly as the fuel, are possible, but suitable membranes are not yet available. In the most recent work, polymer composites containing zirconium phosphates or sulphonated zirconium phenylphosphonate show considerable promise.

1.14 GEL SYNTHESIS AND FUEL CELL MEMBRANES

In one of the most active groups synthesizing fuel cell membranes, Alberti et al. have demonstrated that with the addition of a soluble metal salt, such as alkoxide or carboxylate, in a polar organic solvent to which phosphoric acid and a sulphophenylphosphonic acid have been added, a clear solution is initially obtained. Heating to temperatures above 40°C results in the formation of a mixed derivative such as $Zr(HPO_4)_x(O_3PC_6H_4SO_3H)_{2-x}$ [120, 121]. Many other compositions of the gel may be envisioned. However, the clear solutions have been added to solutions of polymers used as conducting membranes such as Nafion®, polyether ketones and polyvinyl fluoride [120–122]. Thin films of the composites may be cast out and the solvent evaporated at elevated temperatures. In this process, it would seem that many of the arylphosphonates we have described here may also be utilized in this way with or without the addition of phosphoric acid. The process may also be utilized with porous membranes where the pores are filled with the clear solution and the solvent evaporated.

This field continues to be highly active. One of the major problems faced is the high cost of Nafion, and recently, a major increase in its price was installed. Thus, much activity is based upon membrane materials other than Nafion. Alberti et al. found that a sulphonated poly(ether etherketone) (SPEEK) composite membrane exhibited excellent medium-temperature performance at high relative humidity (75%) and 160°C at 4×10^{-2} S cm^{-1}. Subsequently, ZrP or a combination of Zr and Ti phosphates was added [123, 124]. The search for new materials and compositions is an active one as attested to the many recent publications.

We will provide two recent examples. Lee et al. developed a new process for the preparation of nanoparticles of α-ZrP, ZrSPP [$Zr(O_3PC_6H_4SO_3H)_2$], and zirconium sulphate, $Zr(SO_4)_2 \cdot 4H_2O$ [125]. A zirconium oxide powder was prepared by hydrolysis and condensation of zirconium butoxide in isopropanol in the presence of acetylacetone. HNO_3 was added, and after stirring to homogenize the mixture, it was left standing for 6 h. The powder was recovered and dried at 80°. The oxide was then converted to ZrP in 2 M H_3PO_4 at 80°C and to sulphophosphonate by treatment with sulphuric acid. The oxide was also treated separately to obtain the sulphate

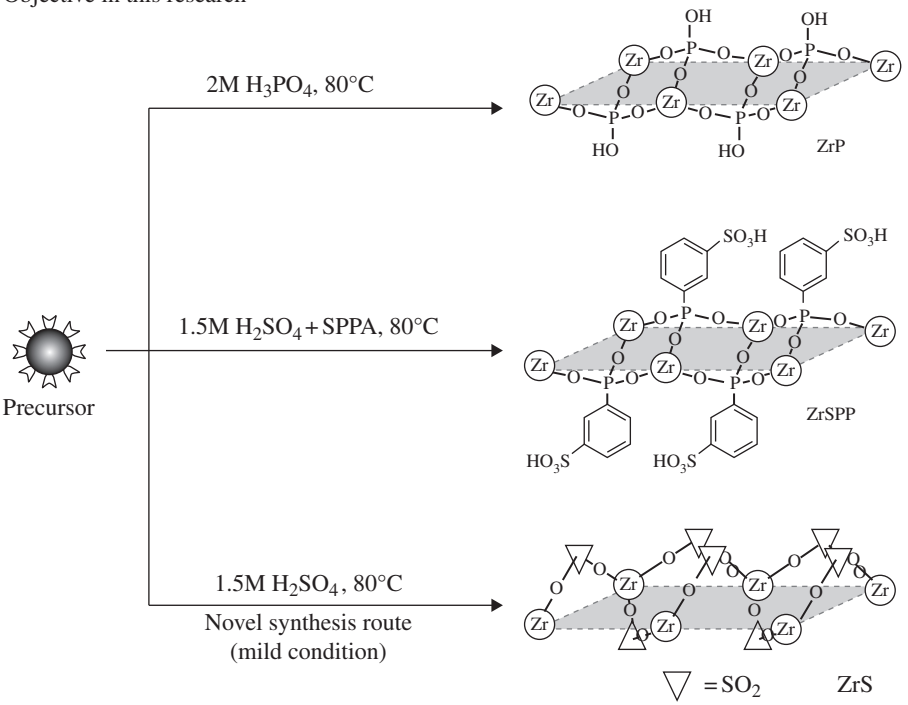

FIGURE 1.26 The novel mild synthesis routes to ZrP, ZrSPP and ZrS from the same precursor at 80°C under mild acidic conditions (Taken from: *J. Mater. Chem.* 2010, *20*, 6239–6244; DOI: 10.1039/C0JM00130A).

(Figure 1.26). The authors claim that this mild method of preparation allows the oxide products to be dispersed in polymer electrolytes at a very high loading with subsequent conversion to the Zr compound conductors. This paper also contains an excellent list of references.

It is pointed out by Pica et al. [126] that Nafion membranes filled with ZrP and other inorganic fillers 'represent the best compromise between chemical stability and proton conductivity but suffer from a relatively low mechanical stability'. However, it is pointed out that a new perfluorosulphonic acid compound that has shorter side chains exhibits a higher crystallinity at a given equivalent weight. This means that for a lesser mass, it may be possible to have high stability for the membrane. Therefore, this new shorter-chain perfluorosulphonate was filled with different amounts of ZrP nanoparticles by solution casting. The membrane exhibited somewhat lower conductivity but an improvement in mechanical properties up to 10 wt% of ZrP [126].

In spite of all the fine research that has been carried out, an ideal PEMFC membrane has not yet been forthcoming. An ideal situation would be to replace platinum with a less expensive catalyst but also more importantly one that would

be uninfluenced by carbon monoxide. Then research could concentrate on membranes that have the necessary proton conductivity together with the required mechanical properties.

1.15 ELECTRON TRANSFER REACTIONS

In our initial attempts at carrying out electron transfer reactions, we found that the intercalation of electron donors between the layers of α-ZrP was a difficult task. Therefore, we utilized zirconium phosphate sulphophenyl phosphonate, (ZrPS) $Zr(HPO_4)(O_3PC_6H_4SO_3H)$. This compound has an interlayer spacing of 16.1 Å and readily takes up large molecules [113]. Our interest was to quantitatively evaluate the nature of the chemical environment within ZrPS and the rate of diffusion within the interlayer space. In this regard, luminescence quenching studies with $Ru(bpy)_3^{2+}$ intercalated into ZrPS were initiated [127, 128]. It was found that the π–π* bond at 285 nm in aqueous solution of $Ru(bpy)_3^{2+}$ is red shifted to 317–320 nm. The metal-to-ligand charge transfer (MLCT) bond is also red shifted, the degree of shift depending upon the amount of $Ru(bpy)_3^{2+}$ intercalated. These several interactions are enhanced by increased packing of $Ru(bpy)_3^{2+}$ within the layers. Subsequently, the delay kinetics of the self-quenching of $Ru(bpy)_3^{2+}$ was determined. The luminescence decay data indicates that a multiplicity of binding sites is present in ZrPS that can explain the self-quenching.

Methyl viologen (MV^{2+}) was also used as a quenching agent. The MV^{2+} was found to lie flat in the α-ZrP layers. These quenching curves were fit to two models of which Albery's dispersed kinetics model gave very excellent duplication of the decay curves [129].

The importance of photoinduced electron transfer reactions is their interest in photosynthesis and is of practical importance for light energy conversion [130]. A major problem is to achieve long-lived charge separation by inhibiting charge recombination reactions. The idea is to create a system to improve the efficiency of energy storage by preventing rapid back electron transfer reactions [131].

Krishna and Kevan, in trying to place *N*,*N*,*N*′,*N*′-tetramethylbenzidine (TMB) in the α-ZrP layers, only succeeded to cover the surface. Nevertheless, after being photoirradiated by >370 nm visible light at room temperature, the colourless sample turned green and became ESR active, confirming the photoionization of the ZrP–TMB samples. The longer the irradiation, up to one hour, of the samples, the stronger the ESR original. The half-life of the photoinduced TMB^+ is about 10 h at room temperature [131]. This is longer than the half-life in micelles and in amorphous silica.

The problem of solving the intercalation of large molecules into ZrP was subsequently solved by Marti and Colon [132]. They synthesized the θ-ZrP phase as described by Kijima [133]. The theta phase is α-ZrP with 5–6 mol of water between the layers creating a 10.3 Å interlayer spacing [134, 135]. Intercalation of $Ru(bpy)_3^{2+}$ was carried out at room temperature with θ-ZrP in water. After

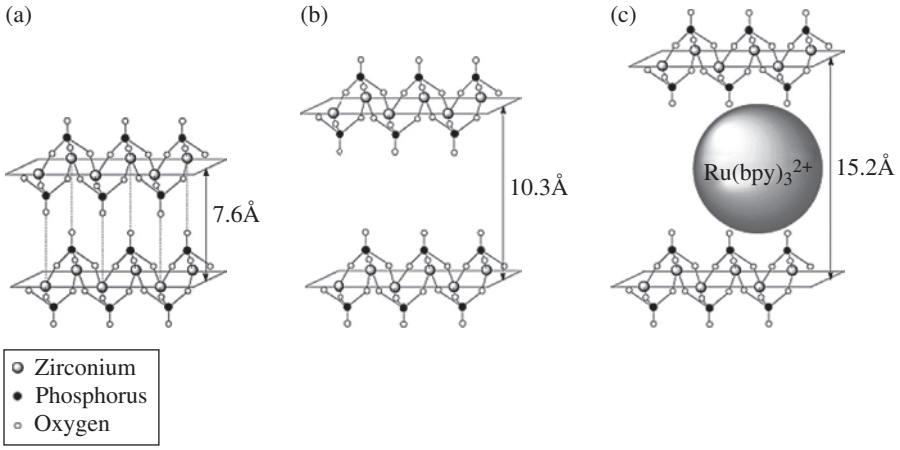

FIGURE 1.27 Idealized representation of three different zirconium phosphate phases: (a) α-ZrP, (b) expanded 10.3 Å phase and (c) $Ru(bpy)_3^{2+}$-exchanged ZrP. Hydrogen atoms and water molecules are not shown for clarity (Taken from: *Inorg. Chem.* 2003, *42*, 2830–2832; DOI: 10.1021/ic025548g).

several days, all the interior sites of the host were occupied by the ruthenium cation as shown figuratively (Figure 1.27).

Subsequently, bis(n^5-cyclopentadienyl) iron(II), ferrocene (Fc), was intercalated into the θ-ZrP layers where it becomes the ferrocenium ion Fc^+. It was found that the intercalated Fc^+ is stabilized within the ZrP layers and remains electroactive. It is capable of oxidizing cytochrome C and quenching the excited state of $Ru(bpy)_3^{2+}$ in aqueous solution [136].

The ability to functionalize the surface of α-ZrP opens up more possibilities for electron transfer reactions. For example, the surface coverage can be changed in an almost unlimited way and electron acceptors bonded to each new surface to assess the electron pathways. Also, it is easy to design electron-conducting polymer composites by adding acceptor groups in the polymer and making the donor in ZrP have functional groups compatible with the polymer.

Our first step in this effort was to intercalate $Ru(bpy)_3^{2+}$ within the layers of θ-ZrP. The platelets were then functionalized with OTS in toluene. There was no significant leaching of the $Ru(bpy)_3^{2+}$ as no change in colour of the solvent was observed. The particles were extremely hydrophobic in character so C_{60} fullerene, also hydrophobic, was used as the acceptor. The luminescence spectra of this system suspended in 1,2-dichlorobenzene with different concentrations of C_{60} from 0 to 300 μm were determined. The results are shown in Figure 1.28.

This result shows that the microenvironment of the intercalated $Ru(bpy)_3^{2+}$ is intact in the interlayer region and was not affected by the surface modification reaction. The inset in Figure 1.28 also shows the Stern–Volmer plot for the quenching of the surface-modified $Ru(bpy)_3^{2+}$/ZrP by C_{60} (inset), indicating an entirely static

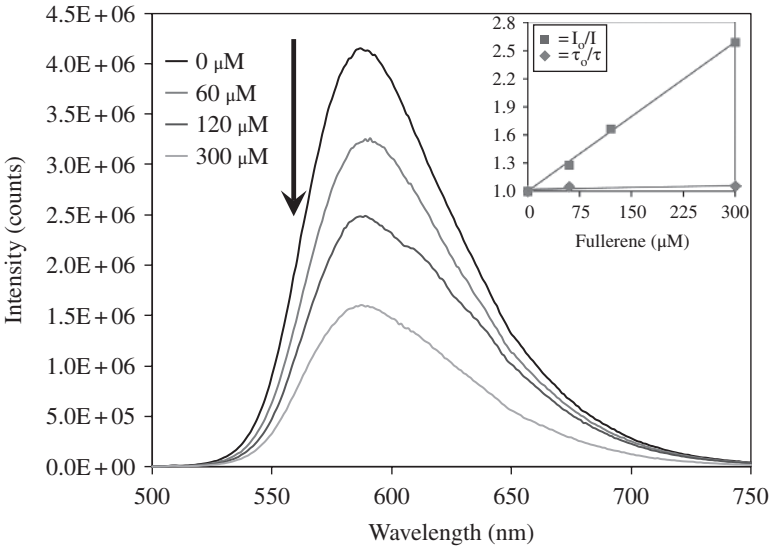

FIGURE 1.28 Luminescent spectra of OTS surface-modified $Ru(bpy)_3^{2+}$/ZrP with different concentrations of C_{60} in 1,2-dichlorobenzene. Inset: Stern–Volmer plot for the quenching with C_{60} using steady-state fluorescence intensity (squares) and fluorescence lifetime (diamonds). λ_{ex} = 440 nm.

quenching mechanism due to the lack of overlapping Stern–Volmer plots for the steady-state fluorescence intensity and time-resolved lifetime measurements. Based on the Stern–Volmer plots, we obtained a static quenching constant (K_s) value of 9.9×10^2 M^{-1}. These reactions now open a wide gamut of new applications for the well-known and versatile zirconium phosphate family. More experiments on surface modification on ZrP are in progress, especially in pursuit of electron-conducting polymer composites.

It should also be mentioned that Brunet et al. have been studying electron transfer reactions using γ-ZrP as the host material for the electron donors [137].

1.16 DRUG DELIVERY

Inorganic layered nanomaterials are receiving attention for biomedical applications because of their size, structure and shape. Kumar and co-workers reported the intercalation of several proteins and enzymes into ZrP, mostly the γ-phase [138]. They generally used the exfoliation method of encapsulation and reported improvement in stabilization, thermal exposure and activity of the intercalates [139, 140].

Our initial effort in drug delivery was to encapsulate insulin into θ-ZrP [141]. This was done using water as solvent. The pH was kept at three, which imparted a

positive charge onto the insulin molecules and a measure of solubility. A slow ion-exchange process occurs in which a phase with an interlayer spacing of 26.2–29.3 Å is obtained. However, not all of the particles were intercalated, which may have resulted in some of the θ-ZrP reverting to α-ZrP as peaks due to this latter phase appear in the X-ray powder pattern. The insulin-containing particles were roughly 150 nm in length. Release of the insulin takes place in about 30 min at pH 7.4. The main reason for this study was to determine whether an alternative delivery system, oral rather than injection, would serve diabetic patients. The nanoparticles may need some surface coverage to clear the acidity of the stomach but would release slowly once in the bloodstream.

Our current research is centred on the delivery of anticancer drugs directly into the cancerous tumours, avoiding interaction with healthy tissue. To affect this salutary result, we make use of α-ZrP nanoparticles as host for the anticancer agents. This compound can be prepared in a form that readily intercalates between their layers high amounts of the anticancer drugs (ca. 30% w/w), such as cisplatin and doxorubicin, among others, and later releases the drugs under pH stimulus. Under standard biological conditions, ZrP is stable and releases its drug in response to the lower pH of the cancer cells and endosomes. Moreover, the extreme conditions of the lysosome and the peroxisomes that are triggered during apoptosis may dissociate the ZrP to form phosphate ion and hydrous zirconia. These products have been found to be biologically benign [142].

It is important to remark that the drug would be biologically inactive while intercalated inside the layers of ZrP and therefore excluded from the external medium and then released and become active once it has reached its target.

The potential for using inorganic layered nanoparticles (ILN) as non-viral vectors and drug carriers has been explored by many investigators [141, 143–146]. However, not many materials have the ability to effectively deliver these anticancer agents in high dosage with minimum damage to healthy tissue. Perhaps the best example is the use of layered double hydroxides [143, 144, 147]. These compounds sorb anions, whereas ZrP is a cation exchanger but also intercalates neutral molecules. There are several advantages to using ZrP over other materials. ZrP nanoparticles have a platelet shape and as we will show can be made small enough to penetrate into cancer cells [146]. ZrP can be compared to highly studied, and widely used in biomedicine, spherical-shaped porous silica nanomaterials [148]. Ferrari et al. have recently referred to spherical nanoparticles as having the worst shape in terms of their margination properties, penetration through vascular fenestrations and adherence to endothelial walls [148–150]. On the contrary, the novel platelet shape of ZrP is very promising to overcome all these disadvantages present in spherical-shaped nanoparticles.

Cisplatin [*cis*-diamminedichloroplatinum(II)] $(NH_3)_2PtCl_2$ and doxorubicin (Adriamycin) are among the most potent anticancer agents approved for use in humans. However, their clinical effectiveness is limited by significant side effects due to lack of specificity and emergence of drug resistance. We believe that this side effect can be significantly avoided if we encapsulate the drugs into the layer of ZrP,

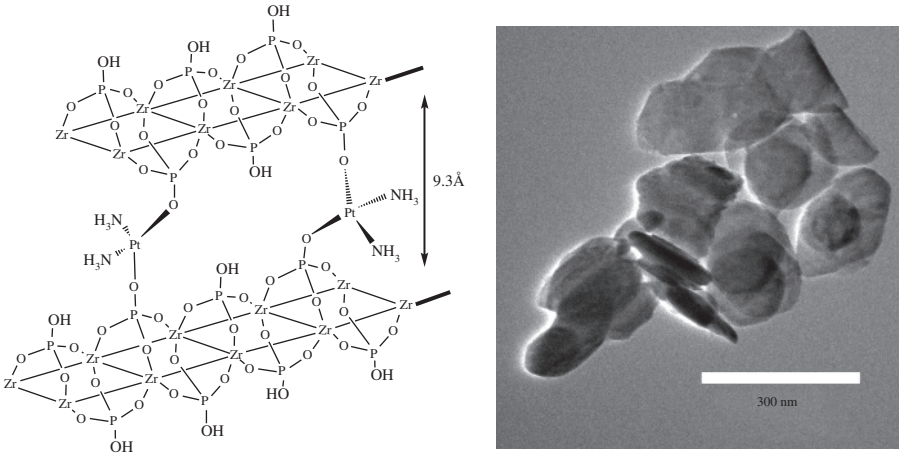

FIGURE 1.29 Idealized representation of cisplatin in the galleries of zirconium phosphate, bonded to the phosphates of the layers in a cross-linked fashion. TEM images of cisplatin–ZrP 1 : 1 intercalation product (Taken from: Diaz, A. Ph. D Thesis, University of Puerto Rico, San Juan 2010).

excluding them from the media until they reach the acidic environment of the tumour. We will describe our preliminary results of the intercalation of both cisplatin and doxorubicin, respectively, into ZrP. The samples were examined by X-ray powder diffraction (XRPD), scanning and transmission electron microscopy, spectroscopic methods and modelling as shown on the left half of Figure 1.29).

In the case of cisplatin, elemental analysis showed that most of the Cl was displaced by the bonding of cisplatin to the layers, producing a new phase with an interlayer distance of 9.3 Å. TEM images show an average particle size of ca. 130 nm [151]. The release profile of the cisplatin–ZrP intercalation product at different pH values in a phosphate buffer shows to be 2.5 times faster at pH 5.4 than at physiological pH. The latter pH approaches the typical pH of the acidic environment of tumour cells, endosomes and lysosomes. The potential inhibition of cell growth by ZrP nanoparticles was evaluated on human breast adenocarcinoma (MCF-7) and T cell lymphoblast-like cell (CEM) lines after a 24 h treatment using the MTT assay procedure. ZrP alone did not affect the viability of MDF-7 and slightly reduced viability of CEM cells. Treatment of CEM cell line with cisplatin reduced the viable cells with an IC_{50} value of 1 μm. However, ZrP–cisplatin (1 : 1) at the concentration of 100 μm reduced 30% of the cell growth.

On the other hand, the intercalation of doxorubicin into ZrP produces a new phase with an interlayer distance of 20.3 Å, A representative model of the ZrP: Cis-platinum phase and its X-ray powder pattern are shown in Figure 1.30. TEM images show an average particle size of ca. 150 nm. The potential inhibition of cell growth by ZrP nanoparticles was evaluated on human breast adenocarcinoma (MCF-7) cell lines after a 24 h treatment using the MTT assay procedure. The cell

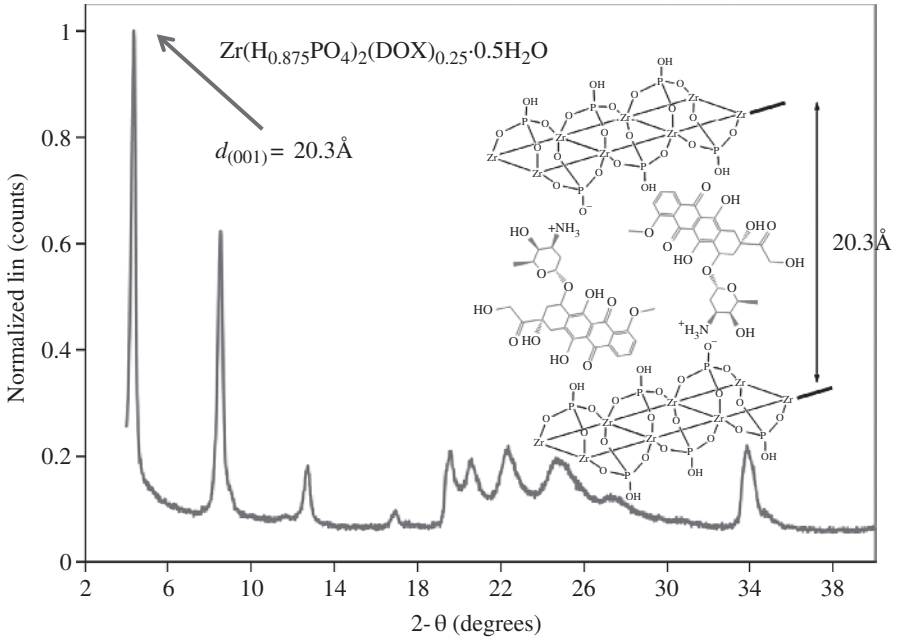

FIGURE 1.30 X-ray powder diffraction (XRPD) of doxorubicin-intercalated ZrP. *Inset:* schematic representation of the intercalation of doxorubicin into α-ZrP by direct ion exchange; the image shows the intercalation of doxorubicin between the layers of ZrP causing the swelling of the particles, forming a new phase with an interlayer distance of 20.3 Å (Modified from: *Chem. Commun.*, 2012, *48*, 1754–1756; DOI: 10.1039/C2CC16218K).

TABLE 1.6 Cell viability assay for doxorubicin in solution and doxorubicin ion exchanged into ZrP

		IC_{50}		
Cell line	Time (h)	Doxorubicin (nM)	ZrP–doxorubicin (nM)	Improvement
MCF-7	24	91.6	31.4	~3×
	48	7.9	2.2	~4×
MDA-MB-231	24	1740	830	~2×
	48	523	199	~3×
	96	2.2	0.8	~3×

viability reveals that the doxorubicin–ZrP intercalation product exhibited a significant higher cytotoxicity than the free doxorubicin. The IC_{50} value for the doxorubicin–Zr nanoparticles (31.41 nM) was found to be ca. 3 times lower than free doxorubicin (91.64 nM). Confocal images show the uptake of the ZrP loaded with doxorubicin into the cell within the first 60 min of incubation (Table 1.6). The

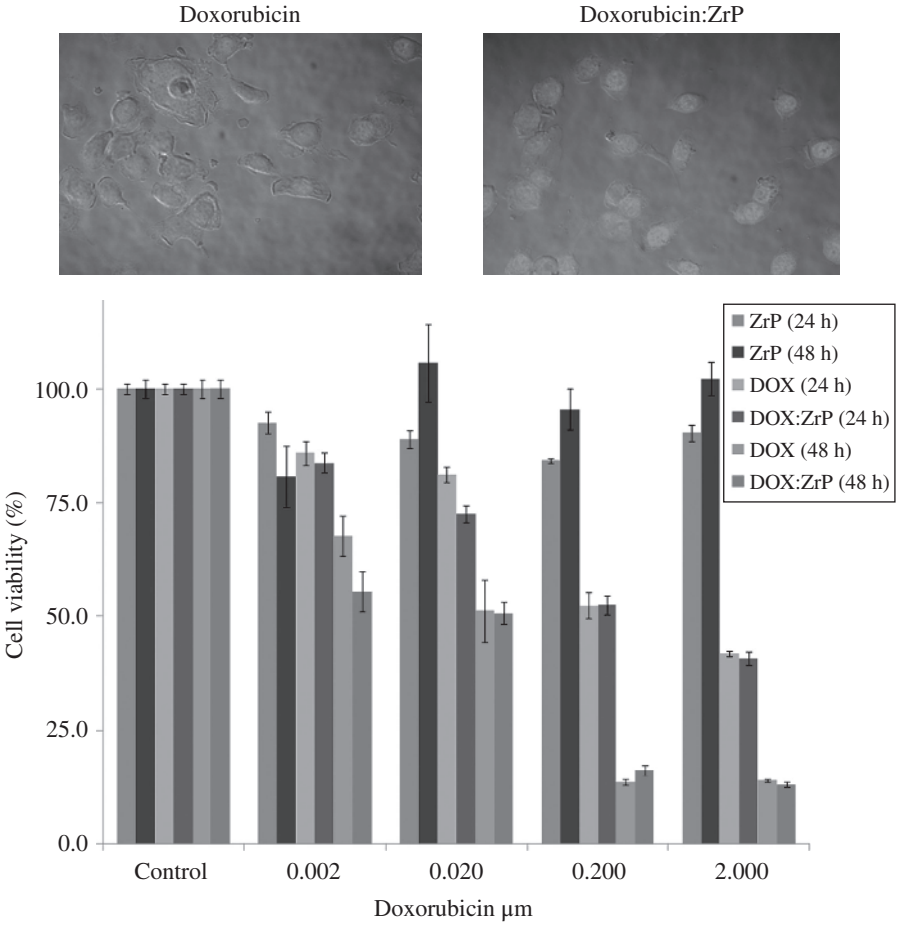

FIGURE 1.31 CLSM images and MTT results in breast cancer cells; top panels show CLSM images of MCF-7 cells treated with DOX (left) and DOX:ZrP (right) nanoplatelets showing the higher uptake of the DOX:ZrP nanoplatelets into the cells. The bottom panel shows MTT assay results in MCF-7 cell lines at 24 h and 48 h of exposure of DOX:ZrP, with their respective controls ($n = 3$, $p < 0.05$ for both 24 h and 48 h of exposure). (Modified from: *Chem. Commun.*, 2012, *48*, 1754–1756; DOI: 10.1039/C2CC16218K, Top panels and Nanoscale, 2013, *5*, 2328–2336. Ref. 151 for bottom graph).

drug release curves are shown in Figure 1.31, and the cellular uptake as revealed by confocal microscope is shown in Figure 1.32.

These results are sufficiently optimistic to consider carrying out *in vivo* studies. In addition, the surfaces require functionalization in order to protect the

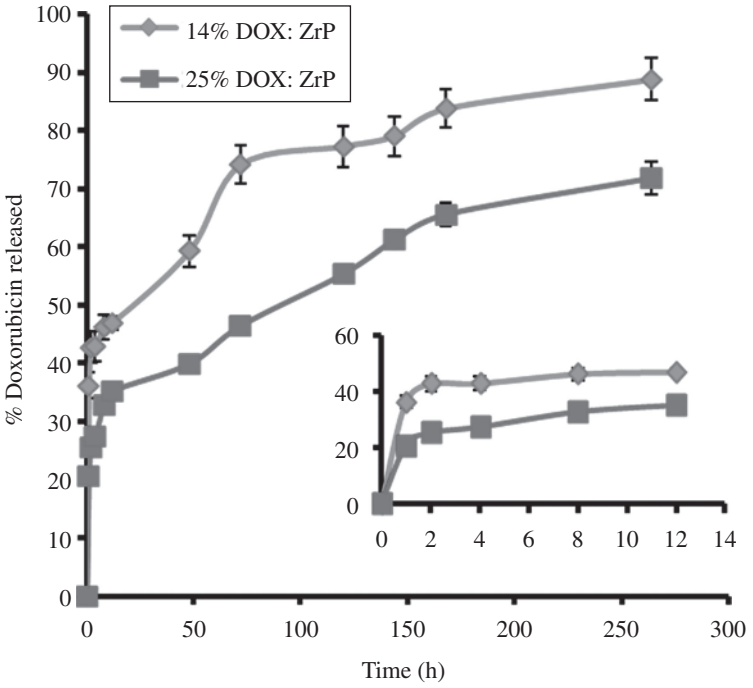

FIGURE 1.32 *In vitro* release profile of doxorubicin (DOX) from different loading level of DOX:ZrP NPs. Drug release study was performed at 37 °C in *simulated body fluid (SBF) pH 7.4*, under shaking (100 rpm) Mean ± SD, $n=3$. (Taken from: *Nanoscale*, 2013, *5*, 2328–2336; DOI: REF. 151, 10.1039/C3NR34242E).

drug from premature release. This we are doing given the fact that the surface layers of ZrP are amenable to forming bonds with such a great array of compounds.

1.17 CONCLUSIONS

We have now completed our excursion through α-ZrP chemistry from its beginnings to the present. But this excursion did not carry us completely through the length and breadth of the subject. We did not include sensors and biosensors, flame retardants, antibiomaterials, and so on. In addition, highly porous forms have been prepared that improve catalytic activity, sorption phenomena and other useful applications. Even after almost 50 years of study, the story is not complete. If we add to this story a similar one for γ-ZrP, also first prepared by the senior author, an equivalently varied and important narrative would obtain. As a start, the reader may wish to consult the excellent review article by Bruno Bujoli et al. [152].

REFERENCES

1. Kraus, K. A., Phillips, H. O. *J. Am. Chem. Soc.* **1956**, *78*, 694.
2. Kraus, K. A., Phillips, H. D., Carlson, T. A., Johnson, J. S. In *Proc. Second Int. Conf.*, United Nations, **1958**, p. 1832.
3. Clearfield, A., Stynes, J. A. *J. Inorg. Nucl. Chem.* **1964**, *26*, 117.
4. Clearfield, A., Smith, G. D. *Inorg. Chem.* **1969**, *8*, 431.
5. Troup, J. M., Clearfield, A. *Inorg. Chem.* **1977**, *16*, 3311.
6. Clearfield, A., Thomas, J. R. *Inorg. Nucl. Chem. Lett.* **1969**, *5*, 775.
7. Sun, L., Boo, W. J., Sue, H.-J., Clearfield, A. New *J. Chem.* **2007**, *31*, 39.
8. Pica, M., Donnadio, A., Capitani, D., Vivani, R., Troni, E., Casciola, M. *Inorg. Chem.* **2011**, *50*, 11623.
9. Trobajo, C., Khainakov, S. A., Espina, A., Garcia, J. R. *Chem. Mater.* **2000**, *12*, 1787.
10. Alberti, G. *Acc. Chem. Res.* **1978**, *11*, 163.
11. Kaschak, D. M., Johnson, S. A., Hooks, D. E., Kim, H.-N., Ward, M. D., Mallouk, T. E. *J. Am. Chem. Soc.* **1998**, *120*, 10887.
12. Clearfield, A., Ed. *Inorganic Ion Exchange Materials*; CRC Press, Boca Raton, FL, **1982**.
13. Clearfield, A., Troup, J. M. *J. Phys. Chem.* **1970**, *74*, 2578.
14. Clearfield, A., Jirustithipong, P. Fast Ion Transp. Solids electrodes electrolytes, *Proc. Int. Conf.*, **1979**, p. 153.
15. Jerus, P., Clearfield, A. *J. Inorg. Nucl. Chem.* **1981**, *43*, 2117.
16. Clearfield, A., Saldarriaga-Molina, C. H., Buckley, R. H., Solid-Solid Ion Exchange, II. Zeolites in Proc. Int. Conf. Mol. Sieves, Uytterhoeven, J. B., Ed. Univ. Leuven Press, Leuven, Belgium, **1973**, 241.
17. Clearfield, A. *Prog. Intercalation Res.* **1994**, *17*, 223.
18. Clearfield, A., Tindwa, R. M. *J. Inorg. Nucl. Chem.* **1979**, *41*, 871.
19. Alberti, G., Casciola, M., Costantino, U. *J. Colloid Interface Sci.* **1985**, *107*, 256.
20. Sun, L., O'Reilly, J. Y., Kong, D., Su, J. Y., Boo, W. J., Sue, H. J., Clearfield, A. *J. Colloid Interface Sci.* **2009**, *333*, 503.
21. Gordon, A., Better, O. S., Greenbaum, M. A., Marantz, L. B., Gral, T., Maxwell, M. H. *Trans. Am. Soc. Artif. Intern. Organs.* **1971**, *17*, 253.
22. Clearfield, A. *Ind. Eng. Chem. Res.* **1995**, *34*, 2865.
23. Clearfield, A. *Annu. Rev. Mater. Sci.* **1984**, *14*, 205.
24. Clearfield, A., Oskarsson, A., Oskarsson, C. *Ion Exch. Membr.* **1972**, *1*, 91.
25. Clearfield, A., Jahangir, L. M. In *Recent Developments in Separation Science*; Navratil, J. D., Ed., CRC Press, Boca Raton, FL, **1984**, Vol. VIII, Ch.4.
26. Eisenman, G. *Biophys. J.* **1962**, *2*, 259.
27. Kullberg, L. H., Clearfield, A. *J. Phys. Chem.* **1981**, *85*, 1578.
28. Gal, I., Ruvarac, A. *J. Chromatogr. A* **1964**, *13*, 549.
29. Horwitz, E. P. *J. Inorg. Nucl. Chem.* **1966**, *28*, 1469.
30. Moore, F. L. *Anal. Chem.* **1971**, *43*, 487.
31. Shafiev, A. I., Efremov, Y. V., Andreev, V. P. *Radiokhimiya* **1973**, *15*, 265.
32. Shafiev, A. I., Efremov, Y. V., Nikolaev, V. M., Yakovlev, G. N. *Radiokhimiya* **1971**, *13*, 129.

33. Cahill, R., Shpeizer, B., Peng, G. Z., Bortun, L., Clearfield, A. In *Separation of F Elements*; Nash, K. L., Choppin, G. R., Eds., Plenum Press Div Plenum Publishing Corporation, New York, **1995**, p. 165.
34. Burns, J. D., Clearfield, A., Borkowski, M., Reed, D. T. *Radiochim. Acta* **2012**, *100*, 381.
35. Burns, J. D., Morkowski, M., Clearfield, A., Reed, D. T. *Radiochim. Acta* **2012**, *100*, 901.
36. Burns, J. D., Shehee, T. C., Clearfield, A., Hobbs, D. T. *Anal. Chem.* **2012**, *84*, 6930.
37. Khan, A. A., Paquiza, L. *Desalination* **2011**, *265*, 242.
38. Pan, B., Zhang, Q., Du, W., Zhang, W., Pan, B., Zhang, Q., Xu, Z., Zhang, Q. *Water Res.* **2007**, *41*, 3103.
39. Zhuravlev, I., Zakutevsky, O., Psareva, T., Kanibolotsky, V., Strelko, V., Taffet, M., Gallios, G. *J. Radioanal. Nucl. Chem.* **2002**, *254*, 85.
40. Mennan, C., Paterson-Beedle, M., Macaskie, L. *Biotechnol. Lett.* **2010**, *32*, 1419.
41. Wang, Z., Pinnavaia, T. *J. Chem. Mater.* **1998**, *10*, 1820.
42. Chan, C.-M., Wu, J., Li, J.-X., Cheung, Y.-K. *Polymer* **2002**, *43*, 2981.
43. Usuki, A., Kojima, Y., Kawasumi, M., Okada, A., Fukushima, Y., Kurauchi, T., Kamigaito, O. *J. Mater. Res.* **1993**, *8*, 1179.
44. Wang, H., Zeng, C., Elkovitch, M., Lee, L. J., Koelling, K. W. *Polym. Eng. Sci.* **2001**, *41*, 2036.
45. Sue, H. J., Gam, K. T., Bestaoui, N., Spurr, N., Clearfield, A. *Chem. Mater.* **2003**, *16*, 242.
46. Boo, W. J., Sun, L. Y., Liu, J., Clearfield, A., Sue, H. J., Mullins, M. J., Pham, H. *Compos. Sci. Technol.* **2007**, *67*, 262.
47. Sun, L., Boo, W.-J., Liu, J., Clearfield, A., Sue, H.-J., Verghese, N. E., Pham, H. Q., Bicerano, J. *Macromol. Mater. Eng.* **2009**, *294*, 103.
48. Krieger, I. M., Dougherty, T. *J. Trans. Soc. Rheol.* **1959**, *3*, 137.
49. Boo, W. J., Sun, L., Warren, G. L., Moghbelli, E., Pham, H., Clearfield, A., Sue, H. *J. Polymer* **2007**, *48*, 1075.
50. Boo, W. J., Sun, L., Liu, J., Clearfield, A., Sue, H.-J. *J. Phys. Chem. C* **2007**, *111*, 10377.
51. Casciola, M., Alberti, G., Donnadio, A., Pica, M., Marmottini, F., Bottino, A., Piaggio, P. *J. Mater. Chem.* **2005**, *15*, 4262.
52. Hung, Y., Carrot, C., Chalamet, Y., Dal Pont, K., Espuche, E. *Macromol. Mater. Eng.* **2012**, *297*, 768.
53. Brandão, L. S., Mendes, L. C., Medeiros, M. E., Sirelli, L., Dias, M. L. *J. Appl. Polym. Sci.* **2006**, *102*, 3868.
54. Sun, L., Liu, J., Kirumakki, S. R., Schwerdtfeger, E. D., Howell, R. J., Al-Bahily, K., Miller, S. A., Clearfield, A., Sue, H.-J. *Chem. Mater.* **2009**, *21*, 1154.
55. Wang, Z. M., Han, H., Chung, T. C. *Macromol. Symp.* **2005**, *225*, 113.
56. Manias, E., Touny, A., Wu, L., Strawhecker, K., Lu, B., Chung, T. C. *Chem. Mater.* **2001**, *13*, 3516.
57. Hasegawa, N., Okamoto, H., Kawasumi, M., Kato, M., Tsukigase, A., Usuki, A. *Macromol. Mater. Eng.* **2000**, *280–281*, 76.
58. Kim, D. H., Fasulo, P. D., Rodgers, W. R., Paul, D. R. *Polymer* **2007**, *48*, 5308.
59. Chung, T. C. *J. Organomet. Chem.* **2005**, *690*, 6292.
60. Alberti, G., Costantino, U., Környei, J., Giovagnotti, M. L. L. *React. Polym. Ion Exch. Sorb.* **1985**, *4*, 1.

61. Lu, H., Wilkie, C. A. *Polym. Adv. Technol.* **2011**, *22*, 1123.
62. Dal pont, K., Gérard, J. F., Espuche, E. *Eur. Polym. J.* **2012**, *48*, 217.
63. Casciola, M., Capitani, D., Donnadio, A., Munari, G., Pica, M. *Inorg. Chem.* **2010**, *49*, 3329.
64. Pica, M., Donnadio, A., Bianchi, V., Fop, S., Casciola, M. *Carbohydr. Polym.* **2013**, *97*, 210.
65. Sagiv, J. *J. Am. Chem. Soc.* **1980**, *102*, 92.
66. Wasserman, S. R., Tao, Y.-T., Whitesides, G. M. *Langmuir.* **1989**, *5*, 1074.
67. Ruckenstein, E., Li, Z. F. *Adv. Colloid Interface Sci.* **2005**, *113*, 43.
68. Sieval, A. B., Linke, R., Zuilhof, H., Sudholter, E. J. R. *Adv. Mater.* **2000**, *12*, 1457.
69. Haensch, C., Hoeppener, S., Schubert, U. S. *Chem. Soc. Rev.* **2010**, *39*, 2323.
70. Park, J.-W., Park, Y.-J., Jun, C.-H. *Chem. Commun.* **2011**, *47*, 4860.
71. Buriak, J. M. *Chem. Commun.* **1999**, 1051.
72. Ulman, A. *Chem. Rev.* **1996**, *96*, 1533.
73. Herzer, N., Hoeppener, S., Schubert, U. S. *Chem. Commun.* **2010**, *46*, 5634.
74. Díaz, A., Mosby, B. M., Bakhmutov, V. I., Martí, A. A., Batteas, J. D., Clearfield, A. *Chem. Mater.* **2013**, *25*, 723.
75. Ramachandran, R., Paul, W., Sharma, C. P. *J. Biomed. Mater. Res. Part B* **2009**, *88*, 41.
76. de Gennes, P. G. *Rev. Modern Phys.* **1992**, *64*, 645.
77. Zhang, C., Liu, B., Tang, C., Liu, J., Qu, X., Li, J., Yang, Z. *Chem. Commun.* **2010**, *46*, 4610.
78. Ling, X. Y., Phang, I. Y., Acikgoz, C., Yilmaz, M. D., Hempenius, M. A., Vancso, G. J., Huskens, J. *Angew. Chem. Int. Ed. Engl.* **2009**, *48*, 7677.
79. Walther, A., Miller, A. H. E. *Soft Matter.* **2008**, *4*, 663.
80. Du, J., O'Reilly, R. K. *Chem. Soc. Rev.* **2011**, *40*, 2402.
81. Perro, A., Reculusa, S., Ravaine, S., Bourget-Lami, E., Dugutt, E. *J. Mater. Chem.* **2005**, *15*, 3745.
82. Jiang, S., Chen, Q., Tripathy, M., Luijten, E., Schweizer, K. S., Granick, S. *Adv. Mater.* **2010**, *22*, 1060.
83. Binks, B. P., Fletcher, P. D. I. *Langmuir* **2001**, *17*, 4708.
84. Faria, J., Ruiz, M. P., Resasco, D. E. *Adv. Synth. Catal.* **2010**, *352*, 2359.
85. Crowley, J. M., Sheridon, N. K., Romano, L. *J. Electrostat.* **2002**, *55*, 247.
86. Mejia, A. F., Diaz, A., Pullela, S., Chang, Y.-W., Simonetty, M., Carpenter, C., Batteas, J. D., Mannan, M. S., Clearfield, A., Cheng, Z. *Soft Matter.* **2012**, *8*, 10245.
87. Kalman, T. J., Dudukovic, M., Clearfield, A. *Adv. Chem. Ser.* **1974**, *133*, 654.
88. Clearfield, A., Pack, S. P. *J. Catal.* **1978**, *51*, 431.
89. Clearfield, A., Thakur, D. S. *J. Catal.* **1980**, *65*, 185.
90. Clearfield, A. *J. Mol. Catal.* **1984**, *27*, 251.
91. Cheung, H. C., Clearfield, A. *J. Catal.* **1986**, *98*, 335.
92. Cheng, S., Clearfield, A. *J. Catal.* **1985**, *94*, 455.
93. Clearfield, A., Thakur, D. S. *Appl. Catal.* **1986**, *26*, 1.
94. Costantino, U., Marmottini, F., Curini, M., Rosati, O. *Catal. Lett.* **1993**, *22*, 333.
95. Zhao, Y., Li, F., Zhang, R., Evans, D. G., Duan, X. *Chem. Mater.* **2002**, *14*, 4286.

96. Zhang, F., Xie, Y., Lu, W., Wang, X., Xu, S., Lei, X. *J. Colloid Interface Sci.* **2010**, *349*, 571.
97. Khare, S., Chokhare, R. *J. Mol. Catal. A Chem.* **2012**, *353*, 138.
98. Niño, M. E., Giraldo, S. A., Paez-Mozo, E. A. *J. Mol. Catal. A Chem.* **2001**, *175*, 139.
99. Alvaro, V. F. D., Johnstone, R. A. W. *J. Mol. Catal. A Chem.* **2008**, *280*, 131.
100. Poojary, M. D., Hu, H. L., Campbell, F. L., III, Clearfield, A. *Acta Crystallogr. Sect. B Struct. Sci.* **1993**, *B49*, 996.
101. Clearfield, A. in *Metal Phosphonate Chemistry: From Synthesis to Applications*, Clearfield, A.; Demadis, K. Eds. RSC Publ. Cambridge, U.K. **2013**, Ch. 1.
102. Wang, Z., Heising, J. M., Clearfield, A. *J. Am. Chem. Soc.* **2003**, *125*, 10375.
103. Curini, M., Epifano, F., Marcotullio, M. C., Rosati, O. *Eur. J. Org. Chem.* **2001**, 4149.
104. Curini, M., Epifano, F., Marcotullio, M. C., Rosati, O. *Synlett.* **2001**, 1182.
105. Curini, M., Epifano, F., Marcotullio, M. C., Rosati, O., Costantino, U. *Tetrahedron Lett.* **1998**, *39*, 8159.
106. Curini, M., Rosati, O., Pisani, E., Costantino, U. *Synlett* **1996**, 333.
107. Curini, M., Marcotullio, M. C., Pisani, E., Rosati, O., Costantino, U. *Synlett* **1997**, 769.
108. Rosati, O., Curini, M., Marcotullio, M. C., Macchiarulo, A., Perfumi, M., Mattioli, L., Rismondo, F., Cravotto, G. *Bioorg. Med. Chem.* **2007**, *15*, 3463.
109. Curini, M., Rosati, O., Costantino, U. *Curr. Org. Chem.* **2004**, *8*, 591.
110. Alberti, G., Casciola, M., Costantino, U., Levi, G., Ricciardi, G. *J. Inorg. Nucl. Chem.* **1978**, *40*, 533.
111. Casciola, M., Costantino, U. *Solid State Ionics* **1986**, *20*, 69.
112. Clearfield, A., Berman, J. R. *J. Inorg. Nucl. Chem.* **1981**, *43*, 2141.
113. Yang, C. Y., Clearfield, A. *React. Polym.* **1987**, *5*, 13.
114. Alberti, G., Casciola, M., Costantino, U., Peraio, A., Montoneri, E. *Solid State Ionics* **1992**, *50*, 315.
115. Stein, S. E. W., Clearfield, A., Subramanian, M. A. *Solid State Ionics* **1996**, *83*, 113.
116. Kullberg, L. H., Clearfield, A. *Solvent Extr. Ion Exch.* **1989**, *7*, 527.
117. Kullberg, L. H., Clearfield, A. *Solvent Extr. Ion Exch.* **1990**, *8*, 187.
118. Song, C. *Catal. Today.* **2002**, *77*, 17.
119. Hirschenhofer, J. H., Stauffer, D. B., Engleman, R. R., Klett, M. G. *Fuel Cell Handbook, Fourth Edition (DOE/FETC-99/1076)*; Department of Energy, Morgantown, WV, **1998**.
120. Alberti, G., Casciola, M., Massinelli, L., Bauer, B. *J. Membr. Sci.* **2001**, *185*, 73.
121. Alberti, G., Casciola, M. *Annu. Rev. Mater. Sci.* **2003**, *33*, 129.
122. Alberti, G., Casciola, M., Pica, M., Di Cesare, G. *Ann. N. Y. Acad. Sci.* **2003**, *984*, 208.
123. Casciola, M., Alberti, G., Ciarletta, A., Cruccolini, A., Piaggio, P., Pica, M. *Solid State Ionics* **2005**, *176*, 2985.
124. Alberti, G., Casciola, M., Pica, M., Tarpanelli, T., Sganappa, M. *Fuel Cells* **2005**, *5*, 366.
125. Lee, J.-M., Kikuchi, Y., Ohashi, H., Tamaki, T., Yamaguchi, T. *J. Mater. Chem.* **2010**, *20*, 6239.
126. Pica, M., Donnadio, A., Casciola, M., Cojocaru, P., Merlo, L. *J. Mater. Chem.* **2012**, *22*, 24902.
127. Colon, J. L., Yang, C. Y., Clearfield, A., Martin, C. R. *J. Phys. Chem.* **1988**, *92*, 5777.

128. Colon, J. L., Yang, C. Y., Clearfield, A., Martin, C. R. *J. Phys. Chem.* **1990**, *94*, 874.
129. Albery, W. J., Bartlett, P. N., Wilde, C. P., Darwent, J. R. *J. Am. Chem. Soc.* **1985**, *107*, 1854.
130. Kevin, L. *Photoinduced Electron Transfer Part B: Experimental Techniques and Medium Effects*; Elsevier Science Ltd, Amsterdam, **1988**.
131. Krishna, R. M., Kevan, L. *Microporous Mesoporous Mater.* **1999**, *32*, 169.
132. Marti, A. A., Colon, J. L. *Inorg. Chem.* **2003**, *42*, 2830.
133. Kijima, T. *Bull. Chem. Soc. Jpn.* **1982**, *55*, 3031.
134. Clearfield, A., Duax, W. L., Medina, A. S., Smith, G. D., Thomas, J. R. *J. Phys. Chem.* **1969**, *73*, 3424.
135. Alberti, G., Costantino, U., Gill, J. S. *J. Inorg. Nucl. Chem.* **1976**, *38*, 1733.
136. Santiago, M. B., Declet-Flores, C., Díaz, A., Vélez, M. M., Bosques, M. Z., Sanakis, Y., Colón, J. L. *Langmuir* **2007**, *23*, 7810.
137. Brunet, E., Alonso, M., Cerro, C., Juanes, O., Rodriguez-Ubis, J. C., Kaifer, A. E. *Adv. Funct. Mater.* **2007**, *17*, 1603.
138. Kumar, C. V., Chaudhari, A. *J. Am. Chem. Soc.* **2000**, *122*, 830.
139. Bhambhani, A., Kumar, C. V. *Microporous Mesoporous Mater.* **2008**, *110*, 517.
140. Jagannadham, V., Bhambhani, A., Kumar, C. V. *Microporous Mesoporous Mater.* **2006**, *88*, 275.
141. Díaz, A., David, A., Pérez, R., González, M. L., Báez, A., Wark, S. E., Zhang, P., Clearfield, A., Colón, J. L. *Biomacromolecules* **2010**, *11*, 2465.
142. Saxena, V., Diaz, A., Clearfield, A., Batteas, J. D., Hussain, M. D. *Nanoscale* **2013**, *5*, 2328.
143. Choy, J.-H., Kwak, S.-Y., Jeong, Y.-J., Park, J.-S. *Angew. Chem. Int. Ed.* **2000**, *39*, 4041.
144. Yang, J.-H., Han, Y.-S., Park, M., Park, T., Hwang, S.-J., Choy, J.-H. *Chem. Mater.* **2007**, *19*, 2679.
145. Oh, J.-M., Choi, S.-J., Kim, S.-T., Choy, J.-H. *Bioconjug. Chem.* **2006**, *17*, 1411.
146. Diaz, A., Saxena, V., Gonzalez, J., David, A., Casanas, B., Carpenter, C., Batteas, J. D., Colon, J. L., Clearfield, A., Delwar Hussain, M. *Chem. Commun.* **2012**, *48*, 1754.
147. Choi, S.-J., Choi, G. E., Oh, J.-M., Oh, Y.-J., Park, M.-C., Choy, J.-H. *J. Mater. Chem.* **2010**, *20*, 9463.
148. Gentile, F., Curcio, A., Indolfi, C., Ferrari, M., Decuzzi, P. *J. Nanobiotechnology* **2008**, *6*, 9.
149. Decuzzi, P., Lee, S., Bhushan, B., Ferrari, M. *Ann. Biomed. Eng.* **2005**, *33*, 179.
150. Ferrari, M. *Nat. Nanotechnol.* **2008**, *3*, 131.
151. Díaz, A., González, M. L., Pérez, R. J., David, A., Mukherjee, A., Báez, A., Clearfield, A., Colón, J. L. *Nanoscale* **2013**, *5*, 11456.
152. Queffélec, C., Petit, M., Janvier, P., Knight, D. A., Bujoli, B. *Chem. Rev.* **2012**, *112*, 3777.